MITIGATING ICE-INDUCED OFFSHORE WIND TURBINE VIBRATIONS UTILIZING A TMD SYSTEM

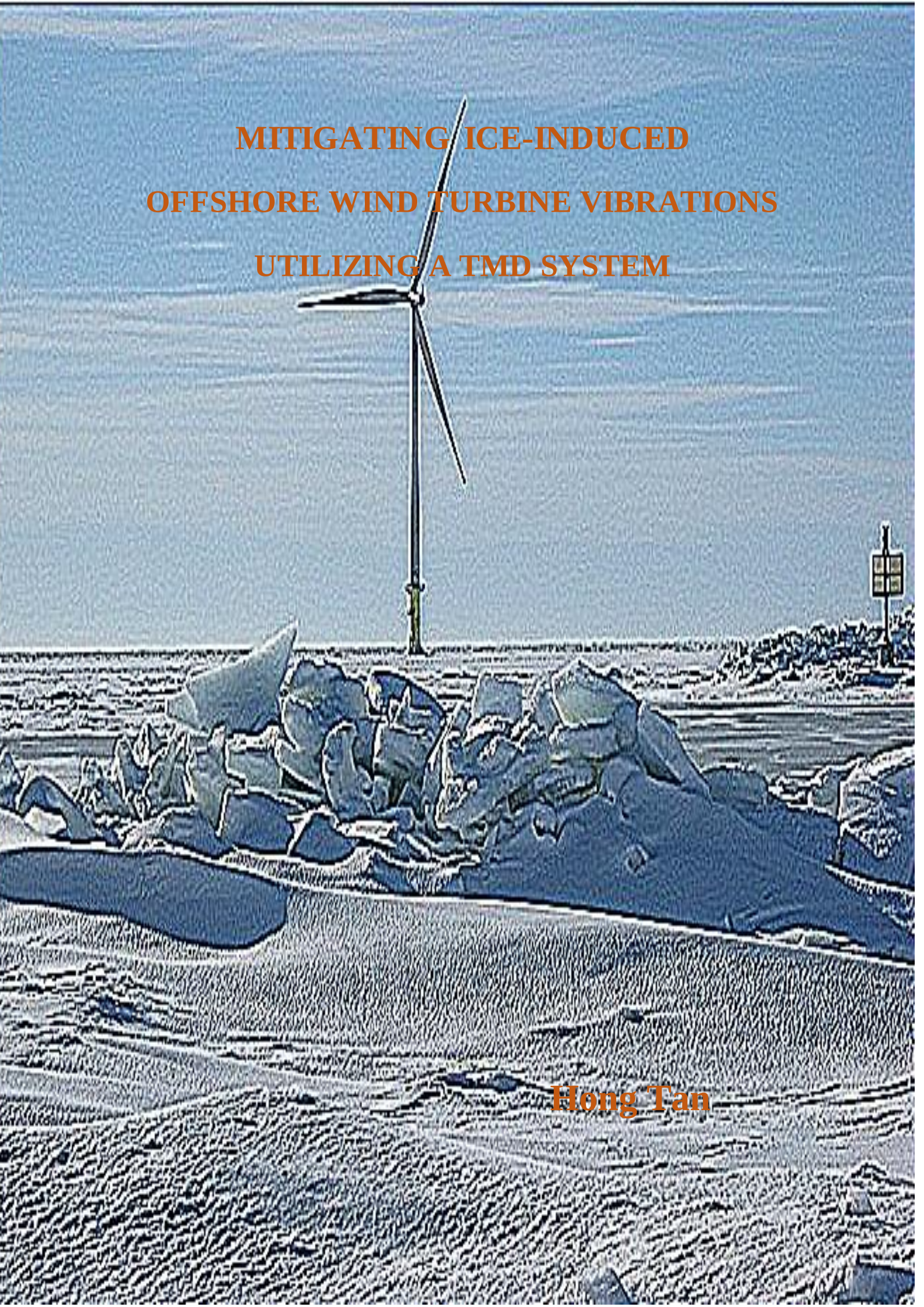

Hong Tan

MITIGATING ICE-INDUCED

OFFSHORE WIND TURBINE VIBRATIONS

UTILIZING A TMD SYSTEM

Author: Hong Tan

Committee: Dr.ir. H. Hendrikse TU Delft-Supervisor

Ir. J.S. Hoving TU Delft-Chairman

Prof.dr. A. Metrikine TU Delft

Dr.ir. F. Pisanó TU Delft

ABSTRACT

In the last few years, increasing attention has been paid to the development of offshore wind industry in ice-infested water region. China as a highly developing country also has a huge ambition in this field. According to the 13th Five-Year Plan (2016-2020) of Chinese government, 5GW offshore wind power grid capacity will be realized before 2020, in which 16% offshore wind turbines will be installed in the Bohai Bay.

Unlike other ice-covered water area, Bohai Bay has a relatively weak ice condition. However, the possible development of ice-induced vibrations is very likely to result in periodic high amplitude oscillations of the structure, which would further contribute to the fatigue of the structure. This thesis mainly aims at investigating the mitigation effects of ice-induced vibrations by means of a tuned mass damper (TMD) device. To achieve this goal, the ice-induced vibrations on the monopile type offshore wind structure have been analyzed numerically.

The structure is first designed and checked based on the environmental data and then it is modeled numerically by a one-dimensional beam. In this process, an ice-crushing model has been implemented for the simulation of ice-induced vibrations on the structure. It has been found that the frequency lock-in can be developed both in the first and second modes of the structure in accordance with the wind speed. Furthermore, the structure may lose contact with the ice in the regime of frequency lock-in due to the wind and current loads when the ice velocity is relatively low.

The TMD model has been applied to investigate the mitigation effects. It predicts that the TMD device can significantly mitigate the ice-induced vibration by absorbing the energy of the structure and 1.5% of tuned mass ratio is shown to be a suitable value for the investigated structure.

Keywords: Offshore wind turbine, Ice-induced vibrations, Tuned mass damper (TMD)

CONTENTS

1

INTRODUCTION

1.1. Background

Due to harsh environmental conditions and high investment, offshore projects in ice-infested water have been seen as one of the frontiers of the offshore industry for a long time. However, in last decades, more attention has been paid to this field in order to meet the increasing energy demands.

The offshore wind industry usually develops wind farms at locations where ice conditions are more moderate, such as the Bohai Bay and the Baltic Sea. Thus, neither icebergs nor multi-year ice ridges will appear in these areas. However, the possible development of ice-induced vibrations caused by first year level ice can still result in periodic high amplitude oscillations of the structure. To ensure the safety of the offshore wind structure, it is important to understand the mechanism of how ice loads generate and how ice and structure interact.

The majority of offshore wind farms are deployed in shallow water, so monopile foundation is a preferred choice for economic reason. Nevertheless, the structural fatigue caused by ice is one of the most significant risks for structures of this type. To effectively solve this problem, the periodic high peak global load caused by the ice-induced vibration has to be considered during the design phase.

As a vertical sided flexible structure, the monopile-type structure can experience three different kinds of ice-induced vibrations during the interaction of ice-structure, namely, intermittent crushing, frequency lock-in, and continuous brittle crushing. This thesis will focus on frequency lock-in, and a numerical model has been built to investigate the mitigation effects of tuned mass damper (TMD).

1.2. Ice-induced vibrations

Ice-induced vibration is the structural vibration which developed by the ice-structure interaction in the ice crushing regime. During the interaction, the large ice load not only pushes the structure to move, but also leads to the crushing failure of the ice at the contact area. This phenomenon has three distinct modes, which depends on the ice velocity, as is shown in Figure 1.1. If the ice speed is slow, intermittent crushing can be developed. When the ice velocity increases to a moderate range, frequency lock-in is likely to be advanced. At high velocities, continuous brittle crushing will occur. The typical structural response and global ice load of these three modes are shown in Figure 1.2. The time dependence saw-tooth patterns oscillation profile is the typical character of intermittent crushing. While in the second regime the structure vibrates at a frequency close to one of its natural frequencies, and the global ice load is locked in this frequency. In the regime of continuous brittle crushing, the structure oscillates at very small amplitude.

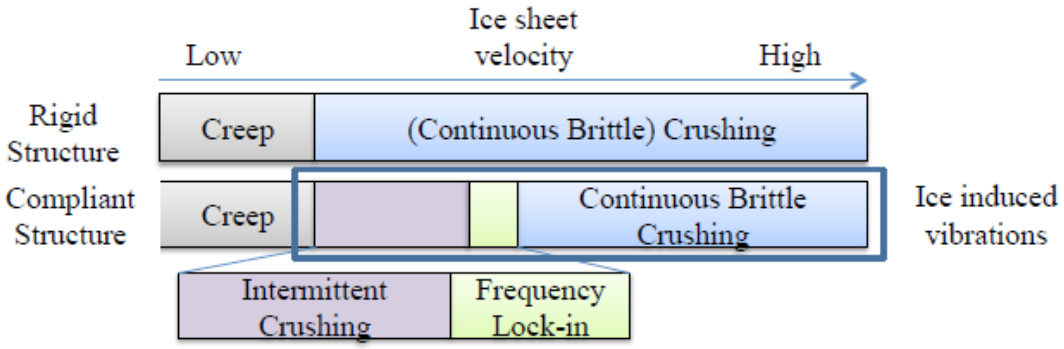

Figure 1.1: Regimes of ice-induced vibration for level ice acting on a vertical sided offshore structure. (H.Hendrikse)

Taking the safety of the structure into account, the regimes of intermittent crushing and frequency lock-in are the most important scenarios that need to be considered during the design phase. Otherwise, it will lead to structural failure or adverse working conditions. For example, a jacket platform and a flare tower were pushed over by level ice in 1969 and 1977 respectively (Yue and Li, 2003).

To solve this problem, several methods have been proposed to mitigate the ice-induced vibrations (Figure 1.3). Applying cones on the structure at its waterline is the most common approach to ice-induced vibration mitigation (Xu et al., 2011),

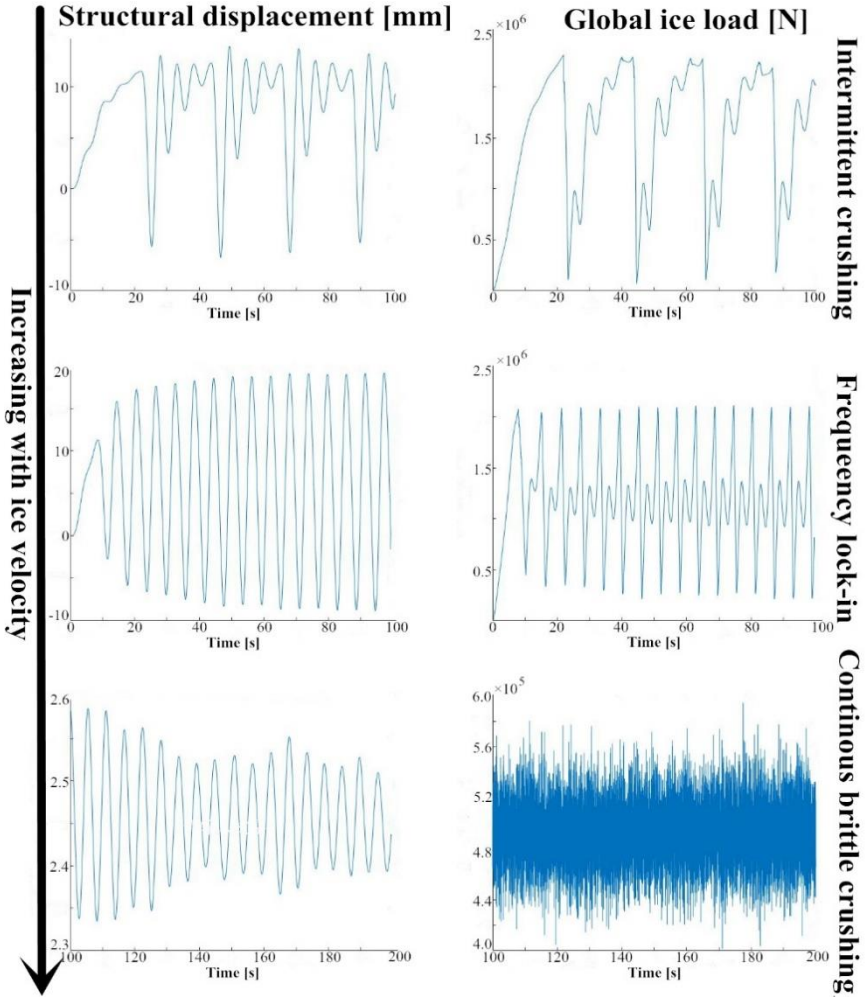

Figure 1.2: The structural displacement and global ice load of three types of ice-induced vibrations.

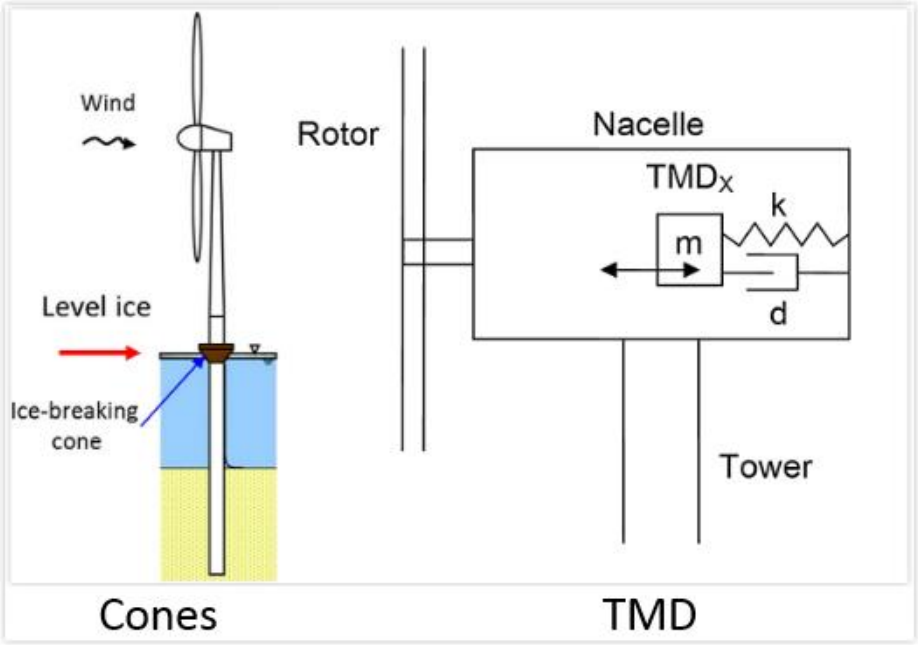

Figure 1.3: Two approaches of mitigating ice-induced vibrations

which can change the failure mechanism of the ice sheet, from crushing to bending, thereby mitigating the ice load as well as ice-induced vibrations. However, this approach cannot avoid leaving periodic iceload on the structure, and will lead to structural vibrations (Yue et al., 2007). Moreover, the additional cost and wave load during the time that no ice is presents is another disadvantage of the cones. In addition, adding cones can lead to the possibility concentration stress in the structure and further cause the local yield failure of the structure. A more feasible and practical approach to mitigate structural vibrations is to apply a tuned mass damper (TMD) on the structure (Yue et al., 2009), which will be investigated numerically in this thesis.

1.3. Historical research on ice-induced vibrations

The ice-induced vibration was first observed in the early 1960s on the drilling platform at the Cook Inlet, Alaska (Peyton, 1968; Blenkarn, 1970). Based on the observation, Peyton first proposed concepts and explanations of intermittent crushing and frequency lock-in, which are still the most frequently adopted mechanisms of ice-induced vibration. Since then, this phenomenon has also been found in some flexible structures such as the lighthouse of the Gulf of Bothnia (Engelbrektson, 1977) and offshore oil jacket platforms in the Bohai Bay (Yue et al., 2001). The explanation of continuous brittle crushing was concluded in the late 1970s (Kry, 1978).

Several models and experiments have been carried out aiming at filling the knowledge gap of ice-structure interaction. The first model which considered the failure length of ice was proposed by Matlock et al. (1969). And then Määttänen (1978) presented a new model which incorporated the negative damping effects. Since then, several experiments were conducted (Määttänen, 1983; Toyama et al., 1983; Tsuchiya et al., 1985), among which, frequency lock-in was first observed to occur over a range of ice velocities. Almost at the same time, Tsuchiya et al., (1985) came up with a new model including both the failure length of the ice and the relation between ice strength and ice loading rate. At the end of the eighties, researchers shifted their focus to slender vertical piles. Kärnä (1992) developed a nonlinear numerical interaction model 'PSS II' which considered the dependence of ice strength on indentation velocity. In the 1990s, Japanese JOIA projects (Saeki et al., 1996) and two full-scale measurements LOLEIF and STRICE on the lighthouse of the Gulf of Bothnia (Schwarz and Jochmann, 2001) made a significant contribution to the data supplement of ice-structure interaction. Since entering the 21st century, several advanced numerical models have been introduced,

including lattice modeling (Dorival et al., 2008), and finite element (FE) techniques with cohesive elements (Gürtner et al. 2010).

The newest phenomenological model for ice crushing was proposed by Hendrikse and Metrikine (2015), which has taken the variation of the contact area into account. The research of this thesis is based on this model.

1.4. Objectives and scope of the thesis

The ice-induced frequency lock-in vibrations can cause high periodic global ice load and structural displacements, which may pose a risk to the safety of the structure. However, vibrations of this type are characterized by periodic oscillation of the structure with a frequency close to one of its natural frequencies. Therefore, it can be mitigated by a tuned mass damper (TMD).

The main objective of this thesis is to investigate the mitigation effect of the TMD device. To achieve this goal, the ice-induced vibrations on a monopile-type offshore wind turbine are first analyzed numerically and then an investigation on the model including the TMD device is conducted. Finally, the simulation results are compared and discussed.

With respect to the structure, it has been simplified to a cylinder in this thesis, which is considered sufficient enough to include all the external loads and capture the structural vibration effects.

1.5. Thesis outline

This thesis contains four main sections. The first part consists of Chapter 2 and Chapter 3, which present the environmental data of this thesis and the preliminary design of the offshore wind structure. The next part is composed of Chapter 4 and Chapter 5, concentrating on the mechanism of ice-induced vibrations, the description of modeling, and related simulation results. The third part, Chapter 6, focuses on the study of mitigation effects of tuned mass damper (TMD). The last part including Chapter 7 and Chapter 8 deals with the conclusion of this thesis and possible further research.

Chapter 2 presents the detailed background and the environmental data of the project area, which will contribute to the structural design and model building in Chapter 3 and Chapter 5 respectively.

Chapter 3 contains the technical data of the wind turbine and the design of the structure, mainly focusing on the definition of structural data, which can be applied to structural modeling in Chapter 5.

In Chapter 4, the definitions of ice crushing regimes of intermittent crushing, frequency lock-in, and continuous brittle crushing will be first given. Then, the ice crushing model (Hendrikse and Metrikine, 2015) is introduced, which will be used for the ice load modeling in Chapter 5.

Chapter 5 makes the first introduction of structural modeling and ice load modeling. In the second part of this chapter, the discussion of different scenario's results has been made. The main purpose of this chapter is to study the ice-induced offshore wind turbine vibrations.

Chapter 6 first illustrates the definition of TMD and then makes a numerical analysis of tuned mass damper deployed structure. This chapter aims to investigate the mitigation effects of ice-induced vibrations by applying a tuned mass damper, and finding the optimized mass value of the TMD.

The possible further research and conclusion are proposed in Chapter 7 and Chapter 8 respectively.

2

ENVIRONMENT DESCRIPTION

2.1. Introduction

Rapid economic growth in China has led to an increasing demand of energy. In addition, the excessive reliance of Chinese energy supply on traditional energy resources makes the problem even worse. Therefore, solving the energy issue has become a priority. China has been trying to develop and utilize new energy resources to satisfy part of the energy demand. Wind energy as a mature technology industry has received considerable attention. However, because of the large population and high occupation rate of the land, Chinese government recently has shifted attention from onshore to offshore wind farm development.

China has a large coastal area with abundant wind energy resources. According to the data from China Meteorological Administration, potential offshore wind power resource of China reaches over 750GW (Gu X., 2008), and Figure 2.1 shows the Chinese offshore wind map. In accordance with the plan, the national offshore wind power grid capacity of China is expected to reach 5GW before 2020, and the expectation of construction capacity is 10GW (China National Energy Administration, 2016), in which 0.8GW capacity is planned to be built in the Bohai Bay. However, this target is far from being reached, and by the end of 2016, only 1.6GW grid capacity was completed. To achieve this goal, a lot of offshore wind projects in China are being prepared.

This thesis focuses on the project in the Bohai Bay, which locates in the northeast of China. The straight coastline, shallow water depth, flat seabed and excellent potential wind energy make Bohai Bay a preferred location for wind farm development. The earliest Chinese pilot offshore wind farm project is deployed here (Zhang et al., 2011). However, the subarctic condition of Bohai Bay can also

result in the presence of ice, which needs to be considered during the design phase of the offshore wind structure.

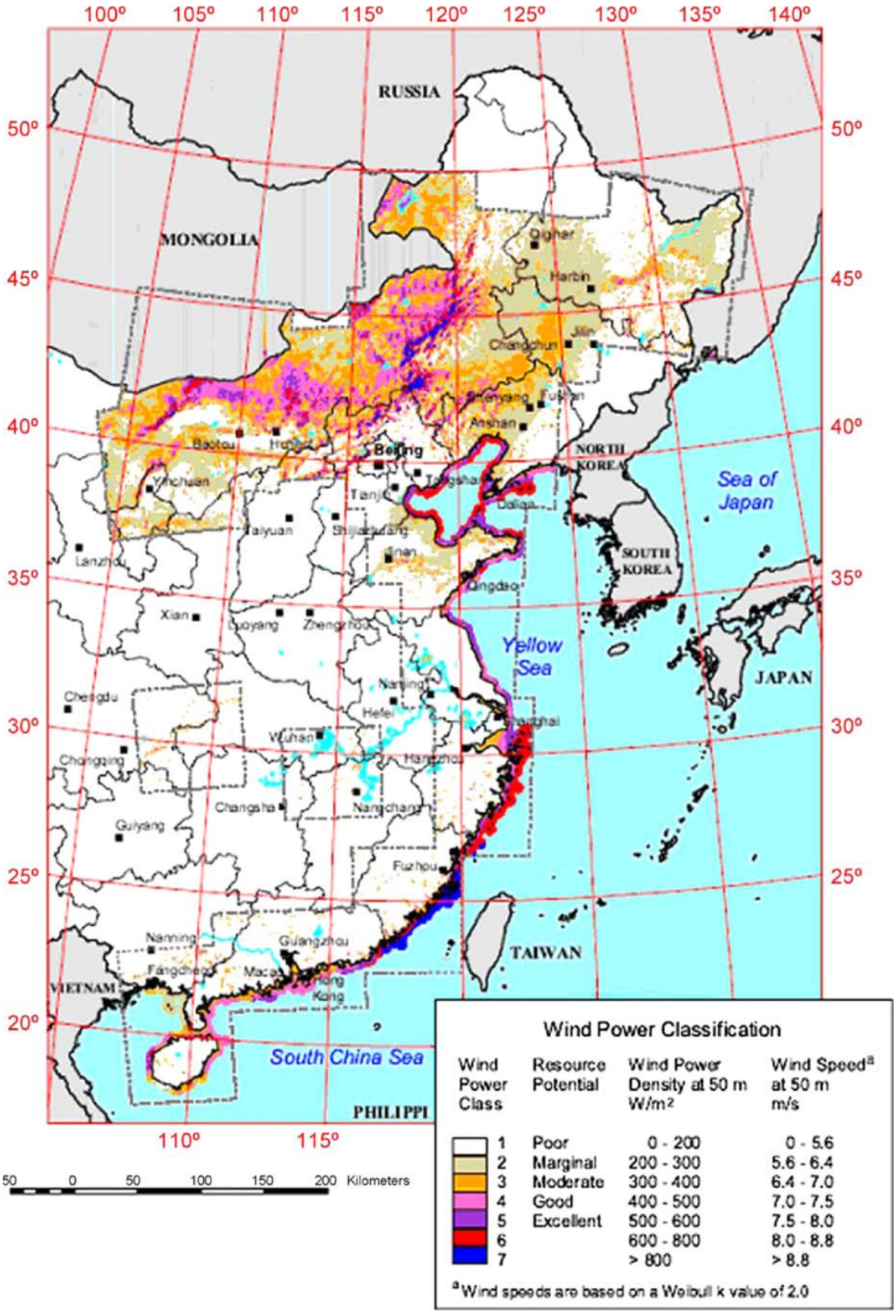

Figure 2.1: Chinese costal wind map

In this chapter, the environmental data of the Bohai Bay are summarized in Section 2.2, and Section 2.3 is a summary of this chapter.

2.2. Environmental data

Bohai Bay is a semi-enclosed continental sea of China with abundant wind energy resource. Several offshore wind farm projects have already been and will be deployed in this area. To study the ice-induced vibrations on the offshore wind structure, the environmental data of Bohai Bay is collected and processed in this section. The sample location of this thesis is 30km offshore, 39° 67'N, 119 ° 67'E. The exact location is shown in Figure 2.2.

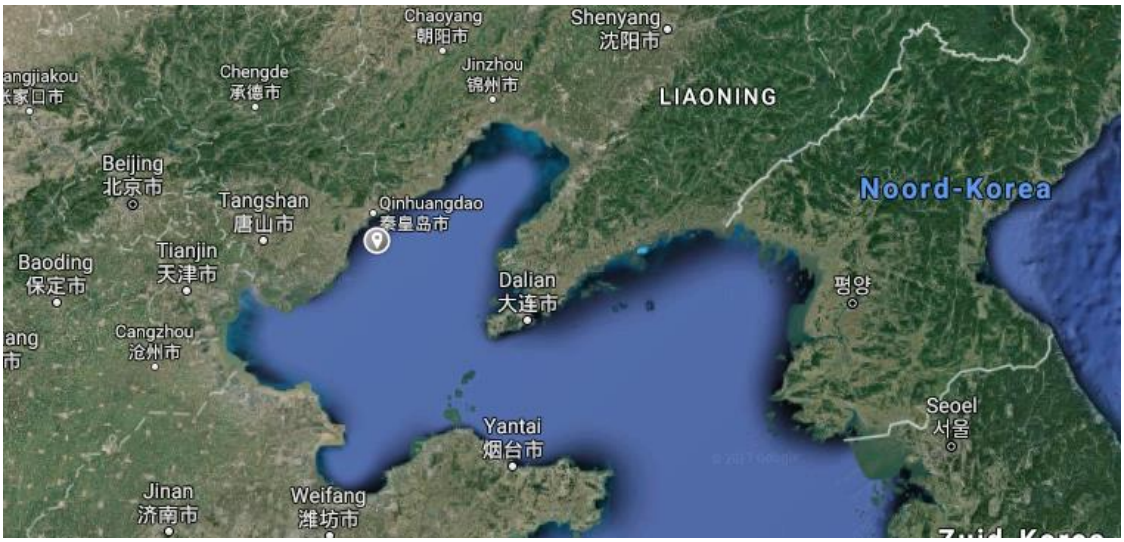

Figure 2.2: The sample location of the monopile-type offshore wind structure

2.2.1. Sea Water

Wang and Wu (2005) summarized the properties of the sea water in Bohai Bay. The key values are listed in Table 2.1.

Table 2.1. Properties of seawater

Description	Value	Dimension
Water density	1025	kg/m³
Water salinity	29	PPT
Water temperature (min/max)	0-27	°C
Air density at 20°C	1.225	kg/m³

2.2.2. Water level

Bohai Bay is a relatively shallow sea, and the mean water depth is only 18 m. Since the project is 30 km offshore, the maximum mean water level in 50 years in this area is 32 m (Pang and Wang, 2010).

2.2.3. Tide and surge

Dealing with the tide and surge data from 1950 to 1990 by applying Gumbel distribution method, the normal and extreme values of this area can be obtained (Wang and Wu, 2005). Table 2.2 has shown the extreme tide and surge values of the project location.

Table *2.2*. Tide and surge data

Description	Dimension	Return Period		
		1 year	50 years	100 years
0.5*tide +surge	m	4.7	5.8	6.38

2.2.4. Wind

The extreme value of wind speed can also be acquired by using Gumbel distribution method. Pang and Wang (2010) presented the 10m height wind speed data in this area, as shown in Table 2.3.

Table 2.*3*. Wind speed data at 10m height

Description	Dimension	Return Period				
		1 year	10 years	25 years	50 years	100 years
1 hour's wind speed	m/s	23.2	28.7	29.6	31.6	32
10 minutes' wind speed	m/s	24.7	30.5	31.5	33	34
1 minute's wind speed	m/s	27.9	34.4	35.5	37.9	38.4
3 seconds' gust speed	m/s	32.8	40.6	41.9	44.9	45.2

2.2.5. Current

Using the same method as described in the wind speed processing, Pang and Wang (2010) got the extreme value of surface current speed in this area. Table 2.4 shows the extreme current speed data.

Table 2.4. Surface current speed data

Description	Dimension	Return Period				
		1 year	10 years	25 years	50 years	100 years
surface current speed	m/s	1.24	1.61	1.75	1.94	2.12

2.2.6. Wave

Based on the wave observation data from 1960 to 1984, Wang and Wu (2005) summarized the extreme significant wave height by using Gumbel distribution method, as shown in Table 2.5.

Table 2.5. Significant wave height data

Description	Dimension	Return Period				
		1 year	10 years	25 years	50 years	100 years
Significant wave height	m	4.45	5.44	6.18	6.8	7.48

2.2.7. Ice

In general, the first day of the ice presence in Bohai Bay is in the period of late November to late December, and the ice will totally melt in March of the second year. The ice-covered season of this area is approximately three months, in which, the most server ice conditions is occur from January to February and during this period, the average ice thickness of Bohai Bay is from 0.1m to 0.5m (Yue et al., 2002), while the normal ice thickness of this project is around 0.2m (Yang, 2009). The ice speed in this area could reach to 1 m/s due to strong seasonal wind and tidal current (Yue et al., 2002). The ice salinity, density, and temperature in this location are summarized by Wang and Wu (2005). Table 2.6 gives the parameters of ice properties in this area. According to the 30 years of temperature data, Wang and Wu (2005) also derived the data of extreme ice thickness, which are listed in Table 2.7.

Table 2.6. Ice properties

Description	Value	Dimension
Ice density	780	kg/m³
Ice salinity	1.43	PPT
Ice temperature (average)	-4.38	°C
Ice speed (max)	1	m/s

Table 2.7. Extreme ice thickness

Description	Dimension	Return Period	
		50 years	100 years
Ice thickness	m	0.67	0.72

2.2.7. Soil

The soil condition in Bohai Bay is quite complicated, and a lot of geotechnical surveys have been initiated here. With so much data of cone penetration tests, Wang and Wu (2005), and Pang and Wang, (2010) analyzed and summarized the distribution of soil layers and soil properties. The specific soil data of this project are listed in Table 2.8.

Table 2.8. Soil properties and the distribution of soil layers

Layer	Soil type	Depth(m)	γ (KN/m^3)	φ(°)	c （kPa）	ε50(%)
1	Clay	0-10.3	10.5	0	105	0.5
2	Clay	10.3-17	10	0	100	0.5
3	Sand	17-26.3	10	35	0	0
4	Clay	26.3-29.2	10	0	105	0.5
5	Clay	29.2-38.2	10.5	0	100	0.5
6	Sand	38.2-44	10	30	0	0
γ is unit weight of soil						
φ is internal friction angle of sand						
Cu is shear strength of clay						
ε50 is the strain of 50% peak stress of clay						

Based on these data, the lateral soil resistance-deflection relationship can be obtained by using API PR 2A_WSD (2000), as given below:

Clay:

Ultimate lateral bearing capacity:

$$P_u = 3c + \gamma X + J\frac{cX}{D}\ [kPa] \quad (X < X_R)$$

$$P_u = 9c\ [kPa] \qquad (X \geq X_R) \qquad (2.1)$$

Where X is the depth below soil surface [mm], the value for the dimensionless empirical constant J is 0.5, and D refers to pile diameter, 7000mm, then the depth below soil surface to bottom of reduced resistance zone

$$X_R = \frac{6D}{\frac{\gamma D}{c}+J} \text{ [mm].} \quad (2.2)$$

The P-Y curve can be generated by Table 2.9.

Table 2.9. The table for generating P-Y curve of clay

$X>X_R$		$X<X_R$	
P/Pu	**y/y_c**	**P/Pu**	**y/y_c**
0	0	0	0
0.5	1	0.5	1
0.72	3	0.72	3
0.72	∞	$0.72X/X_R$	15
		$0.72X/X_R$	∞

In which:

$$y_c = 2.5\varepsilon 50D \text{ [mm]} \quad (2.3)$$

Sand:

Ultimate lateral bearing capacity is the minimum value of:

$$P_u = 1000\gamma H(C_1 H + C_2 D) \ [kN/m]$$

$$P_u = 1000 C_3 D\gamma H \ [kN/m] \quad (2.4)$$

Where H is depth in [m], D is pile diameter=7m, and the coefficient $C_1 = 1.9$, $C_2 = 2.7$, and $C_3 = 29$.

The P-Y curve can be generated by the following equation:

$$P = AP_u \tanh\left(\frac{kH}{AP_u} y\right) \ [kN/m] \quad (2.5)$$

Where, A=0.9, the initial modulus of subgrade reaction k=35 $[kN/m^3]$, and the depth H in [m].

Then, the P-Y curve is obtained. The P-Y curve of these six soil layers is shown in Figure 2.3.

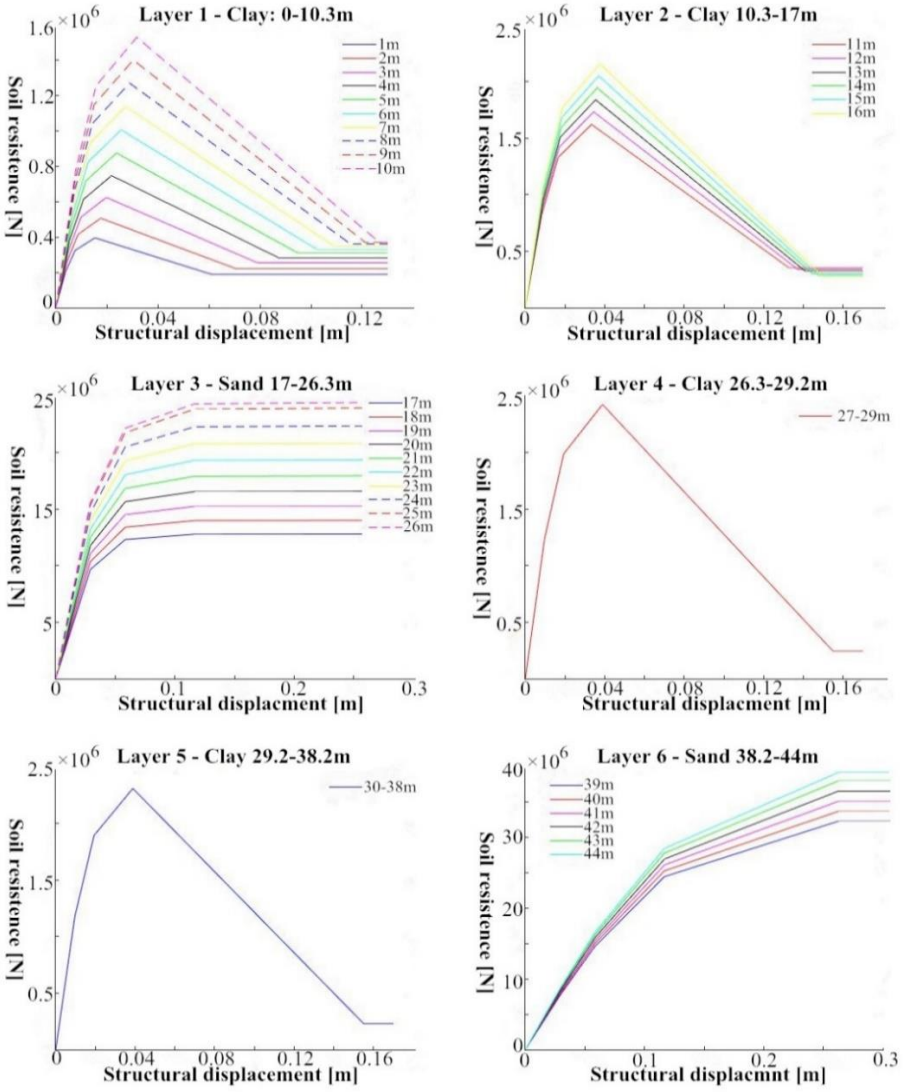

Figure 2.3: The P-Y curve of soil in different soil layers.

2.3. Conclusion

As a combination result of high demands of energy, favorable government policy, and good wind energy potential, the offshore wind energy market in China is experiencing a rapid development.

However, the presence of ice in Bohai Bay may have a big influence on the safety of offshore wind structures in this area. This thesis will focus on a sample project. The basic environmental data has been introduced in this chapter, which will be used in the design of the structure in Chapter 3 as well as the numerical modeling of ice-induced vibrations in Chapter 5.

3

DESIGN OF THE STRUCTURE

3.1. Introduction

The last chapter has introduced the environmental data for the project area and the structure can be designed based on the data. In this thesis, the structure has been simplified to a cylinder, and the diameter and wall thickness of this cylinder are assumed to be known. Therefore, the main purpose of this chapter is to determine the length of the structure.

In this chapter, the load cases for the structural design is presented in Section 3.2, followed with the technical data of the turbine in Section 3.3. Section 3.4 has presented the preliminary design of the structure and Section 3.5 draws a conclusion.

3.2. Load cases

To meet the requirements of structural design, it is necessary to define the load case of this project. The load combination and corresponding values of environmental data are given in Table 3.1 and Table 3.2. It is important to note that the wind speed in Table 3.2 is the 10-minutes wind speed at 10m height.

Table 3.1: Load cases for design purpose

Load Combinations	Surge and Tide	Mean water level	Wind speed	Wave height	Surface current speed	Ice thickness
Unit	m	m	m/s	m	m/s	m
1	50 years	50 years	50 years	50 years	50 years	-
2	50 years	50 years	50 years	-	50 years	50 years

Table 3.2: Vales of extreme values

load combinations for preliminary design						
	0.5*Tide +Surge (m)	**Water Level (m)**	**Wind speed (m/s)**	**Wave height (m/s)**	**Surface current speed (m/s)**	**Ice thickness (m)**
Load Combination	50 years	50 years	50 years	50 years	50years	50 years
Values	5.8	32	33	6.8	1.94	0.67

3.3. Technical data of the turbine

The technical data of the turbine is important for the design of the offshore wind structure. The GE 3.6MW Offshore Series Wind Turbine (General Electric Company, 2005) is selected for this project, which is shown in Figure 3.1 and Table 3.3.

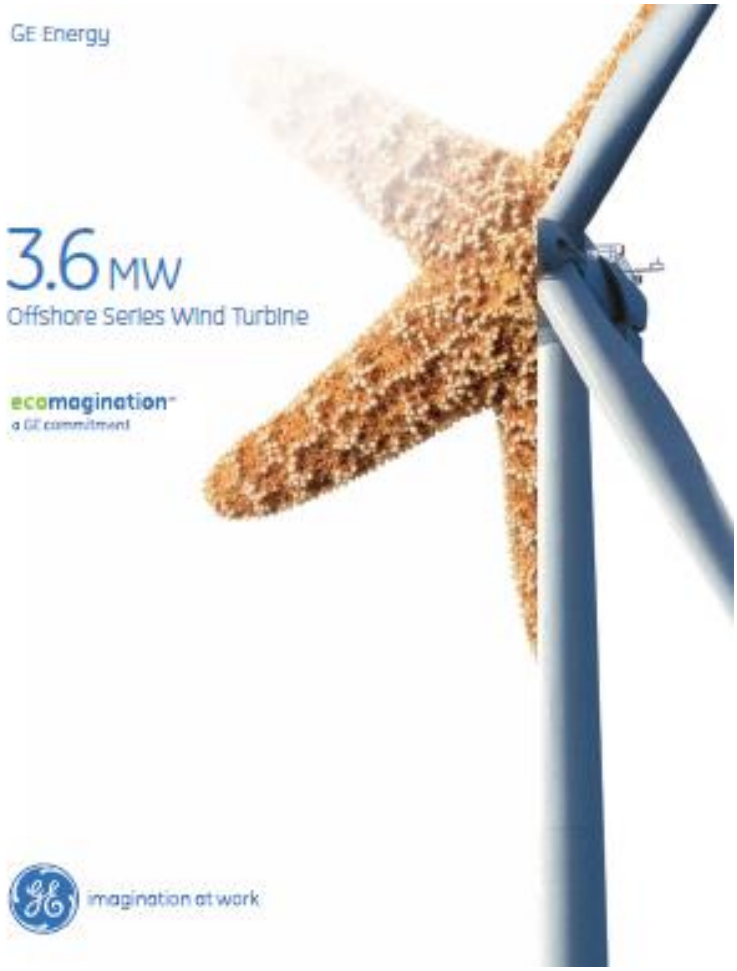

Figure 3.1: GE 3.6MW Offshore Series Wind Turbine

Table 3.3: GE 3.6MW Offshore Series Wind Turbine.

Operating data	
Rated capacity	3,600 kW
Cut-in wind speed	3,5 m/s
Cut-out wind speed	27 m/s
Rated wind speed	14 m/s
Rotor	
Number of rotor blades	3
Rotor Diameter	111m
Swept area	9677 m2
Rotor Speed (variable)	8,5-15,3 rpm
Weight	265000kg

3.4. Technical data of the structure

The structure is simplified to a cylinder. Hence, for numerical modeling, the key technical data are the diameter, wall thickness and total length of the cylinder. In this section, the diameter and the thickness of the cylinder are first given in Section 3.4.1 and Section 3.4.2. According to the data given, the length above the seabed and environmental loads are defined respectively in Section 3.4.3 and Section 3.4.4. In Section 3.4.5, the penetration depth is derived, and Section 3.4.6 has calculated the total length of the structure. Section 3.4.7 has performed the structural check. Finally, in the last part of this section, the structural data have been summarized.

3.4.1. Diameter of the structure

The diameter of the cylinder is assumed to be 7m, neglecting the influence of the marine growth.

3.4.2. Thickness of the structure

According to DNV-OS-J101 (2013), the thickness of the structural can be calculated by the following equations:

$$t = 45 \sim 110 [mm] \tag{3.1}$$

$$D/t = 80 \sim 90 \tag{3.2}$$

Based on these equations, the wall thickness can be calculated as 80mm.

3.4.3. Hub height

The hub height is the length between hub and seabed. The relationships among hub height $z_{hub}\ [m]$, rotor diameter $D_{rotor}\ [m]$, the blade clearance $\Delta z_{clearance}\ [m]$, and the interface elevation $z_{interface}\ [m]$ are shown in Figure 3.2.

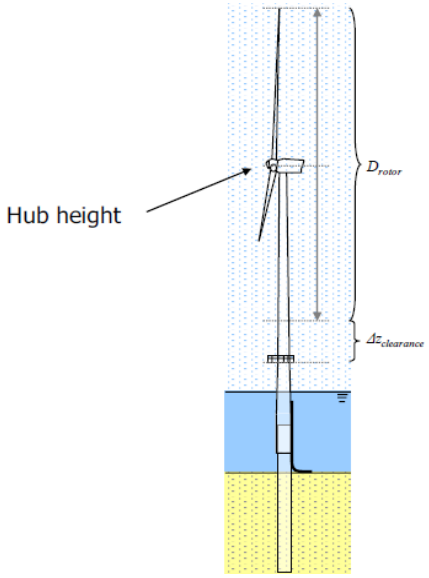

Figure 3.2: Hub height of the monopile-type offshore wind structure

The figure shows that the hub height can be computed through the formulation:

$$z_{hub} = z_{interface} + \Delta z_{clearance} + \frac{1}{2} D_{rotor} \tag{3.3}$$

In which, the interface elevation $z_{interface}\ [m]$ is the length between the interface of platform and sea bed, as shown in Figure 3.3.

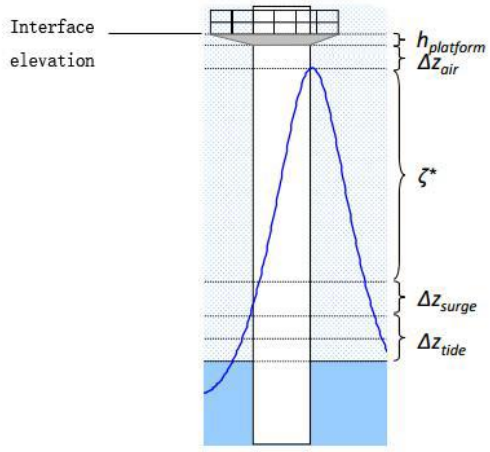

Figure 3.2: Interface elevation of the monopile-type offshore wind structure

According to this figure, the interface elevation can be calculated by the equation:

$$z_{interface} = MSL + \frac{1}{2}\Delta z_{tide} + \Delta z_{surge} + \Delta z_{air} + \zeta^{*} \quad (3.4)$$

Where, MSL is the extreme mean sea level, Δz_{tide} is the extreme tide range [m], the extreme surge range is Δz_{surge} [m], Δz_{air} is the air gap [m], and ζ^{*} is the extreme maximum wave elevation above the still water level [m], which equals to

$$\zeta^{*} = 0.65 * 1.86 * H_{\frac{1}{3}} \quad (3.5)$$

In which, $H_{\frac{1}{3}}$ is the extreme significant wave height [m].

Based on the environmental data and the turbine's data listed in Table 3.4, the hub height can be obtained by substituting these values into equations (3.1) to (3.3).

$$z_{hub} = 112 \text{ [m]} \quad (3.6)$$

Table 3.4: Input parameters for calculating hub height

Parameter	Input Value	Dimension
$\Delta z_{clearance}$	8	m
D_{rotor}	111	m
MSL	32	m
$0.5 * \Delta z_{tide} + \Delta z_{surge}$	5.8	m
Δz_{air}	1.5	m
$H_{\frac{1}{3}}$	6.8	m

3.4.4. Design loads

For the preliminary design, the main purpose of calculating design loads is to get the base shear and overturning moment at the seabed. To realize this goal, four design loads need to be calculated, namely, the wind thrust on the turbine, the wind load on the tower, the ice load/wave load on the pile, and the current load on the pile.

Wind thrust load on turbine:

The thrust load of turbine can be calculated by the Blade Element Momentum (BEM) theory. The thrust load of turbine in different wind speed is shown in Figure 3.3.

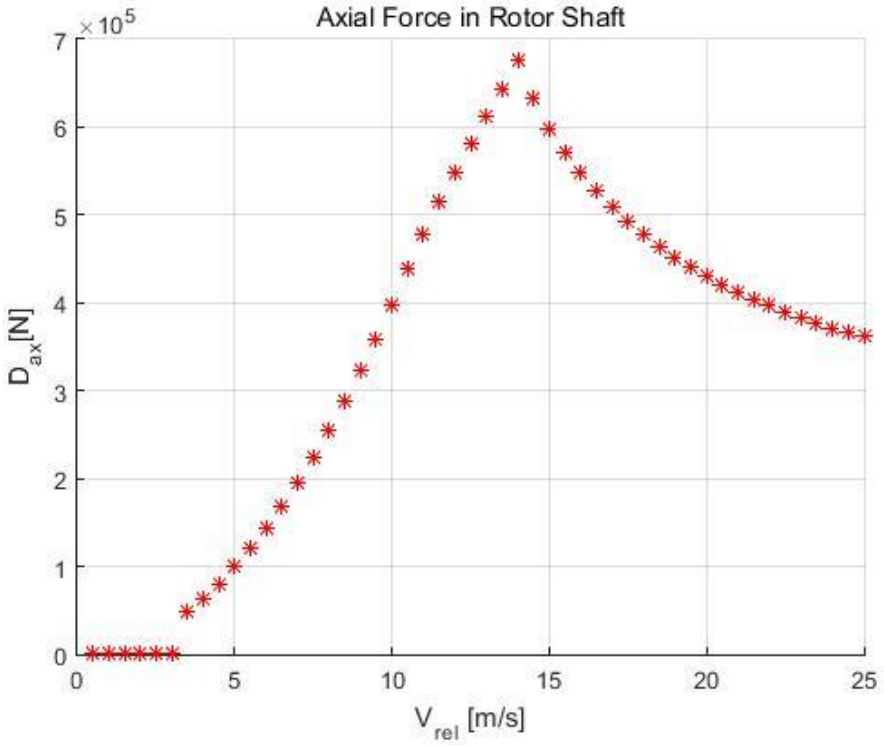

Figure 3.3: The thrust load of turbine in different wind speed

Wind load on tower

The aerodynamic force on tower is calculated by the equation:

$$F_{tower} = \frac{1}{2} \rho_{air} D C_d v^2 l \tag{3.7}$$

Where, ρ_{air} is the density of air [kg/m^3], D is the diameter of the structure [m], C_d is the drag coefficient of the structure [-], and v is the wind velocity and can be obtained by:

$$v = U_{50} \frac{\ln(\frac{z}{z_0})}{\ln(\frac{10}{z_0})} \tag{3.8}$$

In which, U_{10} is the wind speed at 10m high [m/s], and z_0 is the surface reference length [-].

Wave load and Current load

Wave and current loads are those loads that result from water flowing against and around monopile. The hydrodynamic loads considered in this section do include the inertial force and drag force. Morison Equation will be used for calculating hydrodynamic load in this project.

$$F_{Morision} = f_I + f_D = \left(\rho_{water} C_M \frac{\pi D^2}{4} \dot{u} + \frac{1}{2} \rho_{water} C_D D u|u| \right) l \tag{3.9}$$

Where, ρ_{water} is the density of water [kg/m^3], C_M is the added mass coefficient of the structure [-], C_D is the drag coefficient of the structure [-], and u and $\dot{u}$ are the velocity [m/s] and acceleration [m/s^2] of water particle respectively, which can be obtained by:

$$u = u_{wave} + u_{current} \tag{3.10}$$

$$\dot{u} = \dot{u}_{wave} \tag{3.11}$$

The velocity and acceleration of wave can be obtained from potential theory and the current speed can be derived by:

$$u_{current} = u_c \left(\frac{\text{water depth+z}}{\text{water depth}} \right)^{\alpha} \tag{3.12}$$

In which, u_c is the surface current speed [m/s].

Ice load

Ice action is loads exerted on the structure due to ice. For a monopile, the ice normally fails by crushing, so the design ice load for the monopile type structure can be calculated by the equation in ISO-19006 (2010):

$$F_G = P_G hw = C_R \left(\frac{h}{h_1} \right)^n \left(\frac{w}{h} \right)^m hw \tag{3.13}$$

Where, C_R is the ice strength coefficient [MPa], h is the ice thickness [m], and w is the structure width [m].

Based on the load cases and the related environmental parameters, the input parameters are given in Table 3.5. These design loads can be calculated, which are shown in Table 3.6 and Table 3.7. Since all design loads are known, the base shear and overturning moment can be derived by the following equations:

$$F_{shear} = \mathrm{E}_{Factor} * (Thrust + F_{tower} + F_G + F_{Morision}) \quad (3.14)$$

$$M_{shear} = \mathrm{E}_{Factor} * (Thrust * (hub\ height + water\ depth) + \int_0^{hub\ height} F_{tower} * (z + water\ depth)dh + F_G * water\ depth + \int_0^{water\ depth} F_{Morision} * (water\ depth + z)dh) \quad (3.15)$$

Where E_{Factor} is the environmental factor, and the origin of z-axis in the above equations is in the water line and the positive direction is upward direction of the structure.

Table 3.5: Input parameters for calculating design loads

Parameter	Input Value	Dimension
ρ_{air}	1.25	kg/m^3
C_d	1.2	-
D	7	m
l	1	m
z_0	0.0002	-
ρ_{water}	1025	kg/m^3
C_M	2	-
C_D	1.2	-
α	1/7	-
C_R	1.8	Mpa
w	7	m
h_1	1	m
m	-0.16	-
n	-0.366	-
E_{Factor}	1.35	-

Table 3.6: Design loads of load case 1

Thrust+Wind loads+Wave loads +Current loads			
Thrust (MN)	0.91	Mthrust (MNm)	102.12
Fwind (MN)	0.75	Mwind (MNm)	56.56
Fcurrent+Fwave (MN)	4.25	Mcurrent+Mwave (MNm)	82.16
Base Shear(MN)	5.92	Overturning Moment (MNm)	240.85

Table 3.7: Design loads of load case 2

Thrust+Wind loads+Ice loads +Current loads			
Thrust (MN)	0.91	Mthrust (MNm)	102.12
Fwind (MN)	0.75	Mwind (MNm)	56.56
Fice (MN)	9.07	Mice (MNm)	290.1
Fcurrent (MN)	0.68	Mcurrent (MNm)	10.75
Base Shear(MN)	11.41	Overturning Moment (MNm)	459.54

As can be seen from Table 3.6 and Table 3.7, the base shear force and overturning moment of load case 2 are larger than load case 1. Thus for this project, load case 2 will be selected as design load.

3.4.5. Foundation design

Foundation design is mainly focused on the Lateral and Axial stability of the structure. For a monopile-type structure, the axial stability is not a governing factor, thus the deflection of the pile is the main factor that needs to be considered for getting the penetration depth. According to API PR 2A_WSD (2000), the maximum deflection at the pile tip should be smaller than 0.02m and at mud-line less than 0.21m (0.03D). In addition, the rotation at mud-line should be smaller than 0.5°. Based on this, the penetration depth can be calculated, which is 44m. The result of penetration check is shown in Figure 3.4.

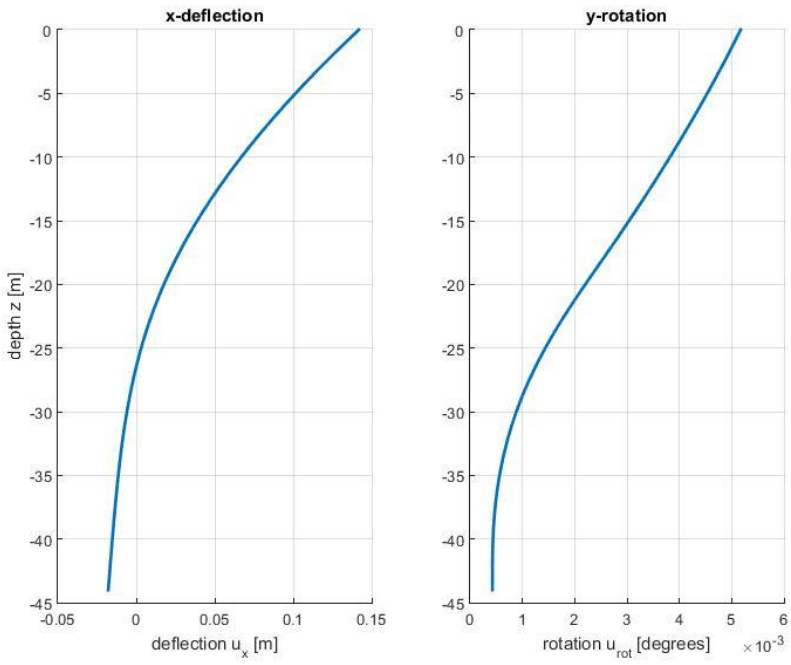

Figure 3.4: The extreme deflection and rotation of the monopile below the seabed

3.4.6. Total length of the structure

After the acquisition of hub height and penetration depth, the total length of the cylinder can be calculated by the following equation:

$$L_{tot} = z_{hub} + L_{penetration} = 156m \tag{3.16}$$

3.4.7. Design check

After the design loads have been obtained, the structure can be checked. In general, for a monopile-type structure, the yield stress, global buckling, and local buckling need to be checked. According to the GL (2012), the structure can be checked by the following equations:

Yield stress check

Yield stress can be checked by the equation below, where N_d and M_d are axial force [MN] and bending moment [MN*m] respectively.

$$\sigma_{vM;d} = \frac{N_d}{A} + \frac{M_d}{W} \leq \frac{f_{yield}}{\gamma_m} \tag{3.17}$$

Global buckling check

Global buckling could be checked by the equation below:

$$\frac{N_d}{\kappa N_p} + \frac{\beta_m M_d}{M_p} + \Delta \mathrm{n} \leq 1.0 \tag{3.18}$$

Local buckling check

Local buckling should be checked by the equation below, where σ_x and σ_φ are axial and circular compressions [MPa] respectively.

$$\left(\frac{\sigma_x}{\sigma_{xu}}\right)^{1.25} + \left(\frac{\sigma_\varphi}{\sigma_{\varphi u}}\right)^{1.25} \leq 1.0 \tag{3.19}$$

The input parameters and checking results are listed in Table 3.8 and Table 3.9 respectively.

Table 3.8: Input for design check

Parameter	Input Value	Dimension
A	1.74	m^2
W	2.26	m^3
f_{yield}	325	Mpa
γ_m	1.1	-
β_m	2	-
k	0.53	-
N_p	514	MN
M_p	667	MN*m
Δn	0.1	-
σ_{xu}	295	MPa
$\sigma_{\varphi u}$	295	MPa

Table 3.9: Results of design check

	Results	Units
Base Shear	11.41	MN
Overturning Moment	459.53	MNm
Yield Stress Ratio	0.7	-
Global Buckling Ratio	0.8	-
Local Buckling Ratio	0.65	-

As can be seen from the table above, the structure is good enough to prevent the structure from global buckling, local buckling and yield.

3.4.8. Summary of the technical data

Since the design check has been carried out, the final structural data of cylinder are summarized, as shown in Table 3.10. Figure 3.5 shows the structural outline as well as the environmental profile.

Table 3.10: Technical data of cylinder

Description	Value	Units
Diameter	7	m
Thickness	0.08	m
Hub Height	112	m
Penetration Depth	44	m
Total Length of Cylinder	156	m

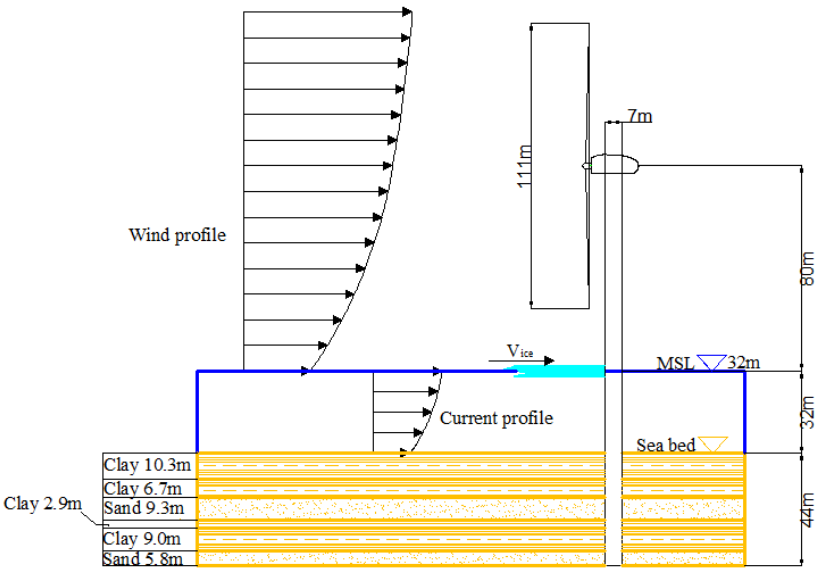

Figure 3.5: Structural outline and the environmental profile.

3.5. Conclusion

The load cases for the design purpose have been presented in this chapter, which have considered the extreme load of the wind, wave/ice, and current. Then the detailed technical data of the turbine have also been summarized. According to these load cases and turbine data, the preliminary design and design loads have been determined. In the last part of this chapter, the structural check is performed.

After the acquisition of all technical data and environmental data, the structure can be modeled numerically by finite difference method in Chapter 5.

4

ICE-INDUCED VIBRATIONS

4.1. Introduction

As is introduced in the First Chapter, ice-induced vibrations can be distinguished to intermittent crushing, frequency lock-in, and continuous brittle crushing. The structural displacement and global ice load of these three regimes of ice-induced vibrations are illustrated in Figure 4.1.

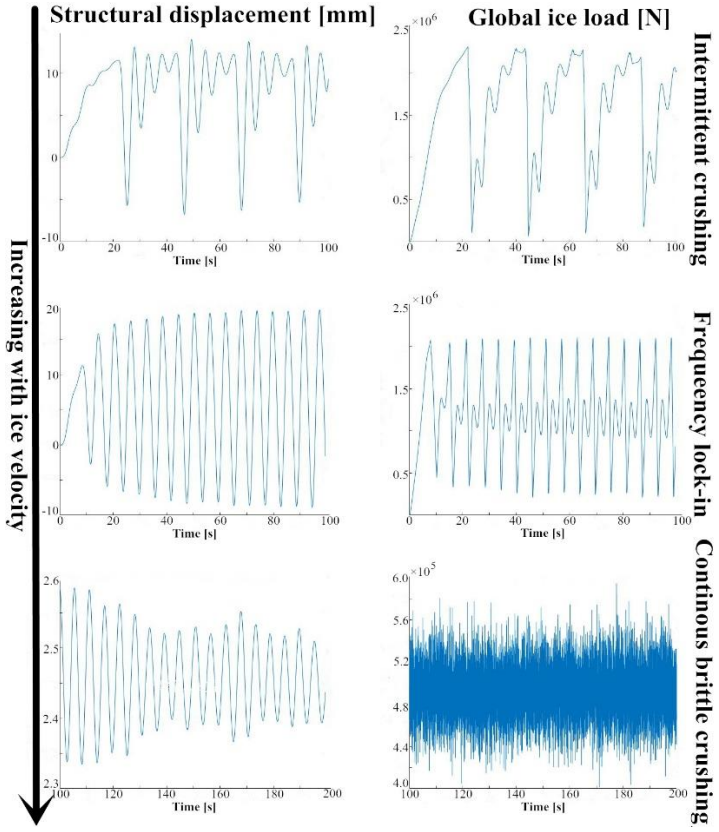

Figure 4.1: The structural displacement and global ice load of three types of ice-induced vibrations.

The occurrence of these three regimes of ice-induced vibrations depends on ice conditions and structural properties. Generally, for low indentation velocities, the intermittent crushing will appear. Then the frequency lock-in occurs at moderate ice speeds. If the ice velocities are high, ice-induced vibrations are continuous brittle crushing.

In this chapter, a detailed introduction of three types of ice-induced vibrations is first given in Section 4.2, followed with the phenomenological ice crushing model (Hendrikse and Metrikine, 2015) in Section 4.3. And the last section makes a summary and conclusion.

4.2. Three types of ice-induced vibrations

According to different indentation velocities, the ice-induced vibrations can be divided into three different regimes, among which, intermittent crushing, frequency lock-in and continuous brittle crushing will be presented in Section 4.2.1, Section 4.2.2 and Section 4.2.3 respectively.

4.2.1. Intermittent crushing

Intermittent crushing occurs at a low ice sheet velocity when it interacts with the flexible structure (Blenkarn, 1970; Kärnä et al., 2003; Sodhi, 2001). In this regime, the global ice load on the structure increases slowly until a significant piece of ice breaks off, due to spatial synchronization of the ice action. Consequently, the load and the displacement of the structure have a saw-tooth profile as a function of time. The example time traces of structural displacement and global ice load are shown in Figure 4.2.

As for a specific structure in the constant ice condition, the frequency of saw-tooth increases with the increase of ice speed until another type of ice-induced vibration occurs (Sodhi, 2001). Furthermore, the oscillation amplitude is determined by the ratio between global ice load and structural stiffness. As a result, this interaction is also referred to as quasi-static interaction (Yue et al., 2002).

The high global peak ice load, as well as the peak structural displacements of intermittent crushing is significantly higher than the continuous brittle crushing, which may lead to severe structural failure. The most well-known case of intermittent crushing is Molikpaq (Figure 4.3), which has suffered severe intermittent crushing on May 12th, 1986 (Jefferies and Wright, 1988). In this case,

a thick first-year ice-floe with several multi-year ice inclusions interacts with the structure by intermittent crushing, endangering the stability of the structure.

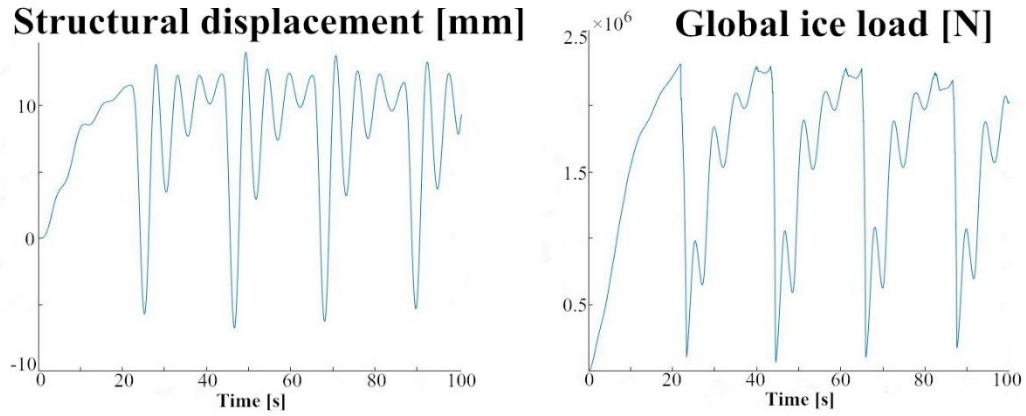

Figure 4.2: Typical time traces of structural displacement and global ice load during intermittent crushing.

Figure 4.3: Molikpaq platform.

4.2.2. Frequency lock-in

Frequency lock-in occurs over a moderate ice speed range for structures with low damping and natural frequencies (Kärnä and Muhonen, 1990; Huang et al., 2007; Yue and Li, 2003), and describes the mode where the failure rate of the ice and the structural motion synchronize both spatially and temporally (lock-in), causing severe structural vibrations. It must be mentioned that the lock-in frequency is not equal to the natural frequency of the structure, nor equal to the breaking frequency of the ice. Actually, it is a natural frequency of the complete system consisting of structure, ice floe and seawater (added mass), which is

slightly below natural frequency of the structure. Example time traces of structural displacement and global ice load during frequency lock-in are shown in Figure 4.4.

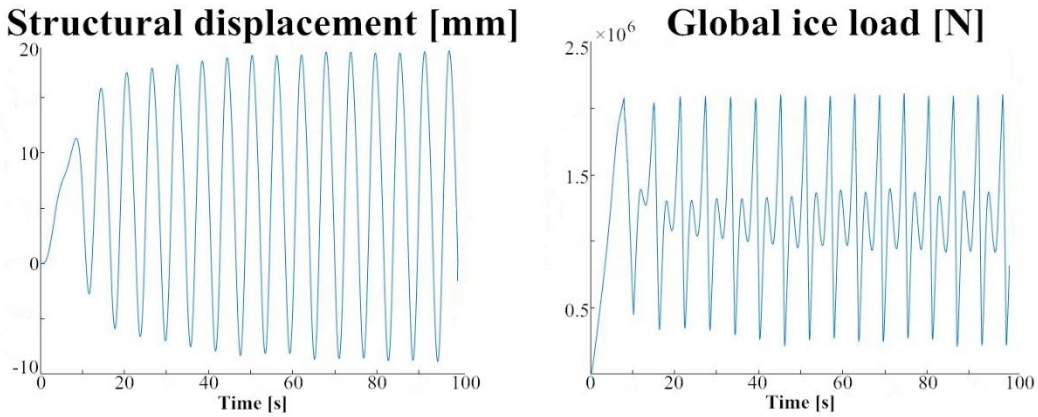

Figure 4.4: Typical time traces of structural displacement and global ice load during first mode frequency lock-in.

As can be seen from the figure above, the displacement of the structure is almost harmonic. During the ice-structure interaction, the ice prevents the structure from moving back until an equilibrium position is reached. Then, the structure starts to move back, the ice fails into powder and reloads on the structure again. Along with this process, the global ice load shows a quasi-random pattern when the indentation velocity is high.

Global ice load and structural displacement of frequency lock-in are also much higher than continuous brittle crushing, which is a potential risk to the safety of the structure. To mitigate this risk, a tuned mass damper has been investigated numerically in Chapter 6.

Distinguish frequency lock-in from other harmonic vibrations

An approximate linear relationship between the structural velocity amplitude and ice sheet velocity has been found by Toyama et al. (1983) and Huang et al. (2007). The relation can be described as:

$$\dot{u}_{max} = \beta * v_{ice} \tag{4.1}$$

According to the results of different experimental campaigns, the value of β varies from 1.0 to 1.5, which means the structure almost moves with the same velocity as the ice when the structural velocity is at its maximum point. This observation can be used to distinguish frequency lock-in from other harmonic oscillations of the structure, such as resonance of the ice-structure system.

4.2.3. Continuous brittle crushing

Continuous brittle crushing occurs at high ice speeds for all flexible structures describing the regime where the structure hardly reacts to the break of the ice. Consequently, there is no spatial or temporal synchronization. The ice breaks up into very small pieces and can be considered to pulverize. The global ice load on and the displacement of the structure has a random profile (white noise) around a roughly constant mean value. The amplitude of vibration of the structure and the maximum ice load are much lower than other two regimes. Example time traces of structural displacement and global ice load during continuous brittle crushing are shown in Figure 4.5.

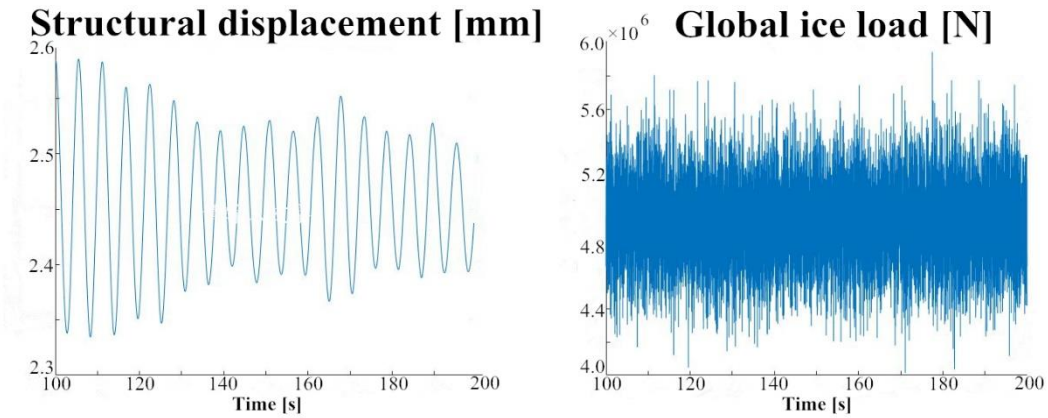

Figure 4.5: Typical time traces of structural displacement and global ice load during continuous brittle crushing.

Because of the insignificant amplitude of both structural displacements and global ice loads, this regime of ice-induced vibration will not threaten the structure.

4.3. Phenomenological ice-crushing model

In this section, a phenomenological ice crushing model (Hendrikse and Metrikine, 2016) will be presented. Figure 4.6 shows an overview of the model. As can be seen from this figure, the structure is modeled as a single-degree-of-freedom oscillator, while the ice sheet is represented by N crushing elements to capture the contact area variation. Each element is represented by an elastic–viscoplastic material with strain hardening, also known as Bingham element. On top of this, an added rear dashpot is included in this model.

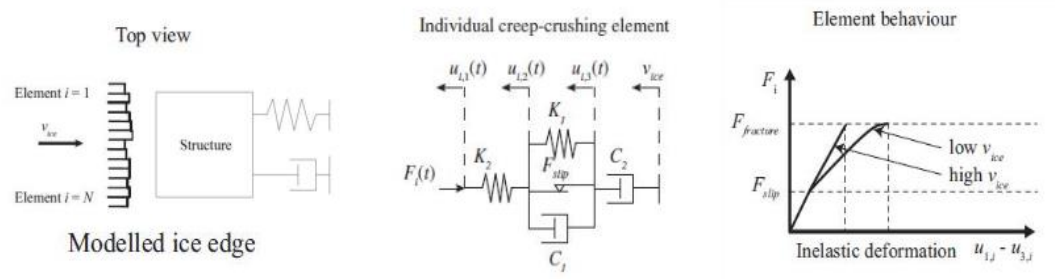

Figure 4.6: Left: Top view of ice sheet edge and structure, in which the ice sheet has been divided into N individual elements. Center: The model of a single ice element in the interface of the ice-structure interaction. Right: Load-displacement curve of ice-element model for different ice speeds, in which $\mathrm{F}_{fracture}$ is the fracture load in front of the element.

Under assumption that the ice sheet velocity can be considered to be constant, and the environmental driving force on the ice sheet and mass losing during the ice-structural interaction can be neglected, the equations of motion for a single element are given by:

$$u_{i,1}(t) = \begin{cases} u_{i,2}(t) & no\ contact \\ u_s(t) & contact \end{cases}$$

$$\dot{u}_{i,2}(t) = \begin{cases} v_{ice} & no\ contact \\ \frac{K_2}{C_2}\left(u_s(t) - u_{i,2}(t)\right) + v_{ice} & contact\ stick \\ \left(\frac{K_2}{C_1} + \frac{K_2}{C_2}\right)\left(u_s(t) - u_{i,2}(t)\right) + \frac{K_1}{C_1}\left(u_{i,3}(t) - u_{i,2}(t)\right) + v_{ice} + \frac{F_{slip}}{C_1} & contact\ slip \end{cases} \quad (4.2)$$

$$\dot{u}_{i,3}(t) = \begin{cases} v_{ice} & no\ contact \\ \frac{K_2}{C_2}\left(u_s(t) - u_{i,2}(t)\right) + v_{ice} & contact \end{cases}$$

Where $u_{i,1} - u_{i,3}$ are displacements of characteristic points of element i [m], u_s represents the structural displacement [m], v_{ice} stands for the velocity of ice sheet [m/s], K_1 and K_2 are the stiffness of the center spring of the element and elastic stiffness of ice respectively $[\mathrm{kg/s^2}]$, C_1 and C_2 are the damping coefficient of the center dashpot of the element and rear dashpot of the element respectively [kg/s], F_{slip} is the sliding force of the element [N], and t is time [s]. Different situations of contact, no contact, contact slip, and contact stick have also been distinguished in equation (4.2).

The global ice load is the sum of ice load of each element that exerts on the structure, which is given by:

$$F_{ice}(t, u_s, \dot{u}_s) = \sum_{i=1}^{N} K_2 \left(u_{i,2}(t, u_s, \dot{u}_s) - u_{i,1}(t, u_s, \dot{u}_s)\right) \quad (4.3)$$

Based on the global ice load F_{ice} [N], the mass of the structure M_s [kg], the structural damping C_s [kg/s], and the structural stiffness K_s [kg/s^2], the equation of motion of structure is given by:

$$M_s\ddot{u}_s + C_s\,\dot{u}_s + K_s u_s = F_{ice}(t, u_s, \dot{u}_s) \quad (4.4)$$

The fracture of ice is set to occur by a critical value δ_{crit} of deformation, which is given by:

$$u_{i,2}(t) - u_{i,1}(t) = \delta_{crit} \quad (4.5)$$

Since, the fracture of the ice occurs, and the original element will be replaced by a new element with the new ice edge position from a uniform distribution $U(u_s - r_{max}, u_s)$, in which r_{max} is the value of maximum offset of the element from the structure.

The initial conditions of structure are defined by $u_s(0)$ and $\dot{u}_s(0)$. The initial position of the front of each element is compensated by elastic deformation and is drawn from a uniform distribution as $U(u_s - r_{max} - \delta_{crit}, u_s)$.

Definition of model input parameters

The twelve input parameters of the model include four clearly defined parameters and eight unknown parameters. The data of the structure M_s, C_s, K_s, and the indentation velocity v_{ice}, are four known parameters. The remaining eight parameters K_1, K_2, C_1, C_2, F_{slip}, δ_{crit}, r_{max}, and N can be defined by eight reference measurements data, which are obtained under the condition of a low aspect ratio between the ice sheet thickness h_{ref} and the structural width d_{ref}. The eight reference data are given in Figure 4.7.

In which, $v_{ref,tans}$ is the transition velocity between global creep and brittle ice behavior [m/s], and $v_{ref,high}$ is the high indentation velocity [m/s] in the regime where the ice deformation is almost purely elastic from which the elastic behavior of ice is defined as a critical value c_{ref}. Four reference load values are defined as the maximum global load at the transition velocity $F_{ref,max}$ [N], the mean global load at an indentation velocity which is twice the transition velocity $F_{ref,mean,2}$ [N], the mean global load at high indentation velocity $F_{ref,mean}$ [N], and the standard deviation of the global load at high indentation velocity $F_{ref,std}$

[N]. $t_{ref,peak}$ is the time moment that peak load occurs in creep at the transition velocity [s], while $f_{ref,peak}$ is the peak frequency in the spectrum of the load [s^{-1}].

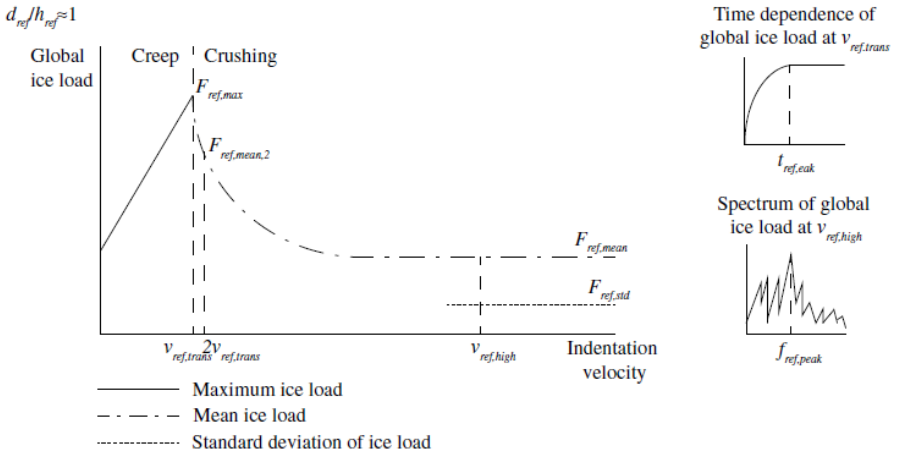

Figure 4.7: Example illustration of input curve of reference measurement data, which can be used to define the input parameters of ice-crushing model.

With all reference measurement data obtained, the input parameters of the model can by derived by the following equations:

$$F_{slip} = c_{ref} K_2 \, \delta_{crit} \tag{4.6}$$

$$F_{ref,mean}(v_{ice}) = N \frac{K_2 \int_0^{t_{fail}} u_{i,2} dt}{\frac{0.5 r_{max}}{v_{ice}} + t_{fail}} \tag{4.7}$$

$$F_{ref,std}(v_{ice}) = \sqrt{N \frac{{K_2}^2 \int_0^{t_{fail}} u_{i,2} dt}{\frac{0.5 r_{max}}{v_{ice}} + t_{fail}} - F_{mean}(v_{ice})^2} \tag{4.8}$$

$$f_{ref,peak}(v_{ice}) = \frac{0.5 r_{max} + \delta_{crit}}{v_{ice}} \tag{4.9}$$

$$F_{ref,max} = N K_2 \, \delta_{crit} \tag{4.10}$$

$$\delta_{crit} = 2 \frac{F_{ref,mean}}{F_{ref,max}} \frac{v_{ref,high}}{f_{ref,peak}} \tag{4.11}$$

$$r_{max} = \frac{2 v_{ref,high}}{f_{ref,peak}} - 2 \, \delta_{crit} \tag{4.12}$$

$$N_{ref} = \frac{\frac{2}{3} {F_{ref,max} F_{ref.mean}}^2 - {F_{ref.mean}}^2}{{F_{ref,std}}^2} \tag{4.13}$$

$$K_2 = \frac{hF_{ref,max}}{h_{ref}N_{ref}\,\delta_{crit}} \tag{4.14}$$

$$N = \frac{d_s}{d_{ref}}N_{ref} \tag{4.15}$$

$$C_2 = \frac{K_2\,\delta_{crit}}{v_{ref,tans}} \tag{4.16}$$

$$F_{ref,mean,2} = N_{ref}\frac{K_2\int_0^{t_{fail}} u_{i,2}(t,2v_{ref,tans})dt}{\frac{0.5r_{max}}{2v_{ref,tans}}+t_{fail}} \tag{4.17}$$

$$t_{ref,peak} = \frac{0.5r_{max}}{v_{ref,tans}} + t_{f1} \tag{4.18}$$

$$u_{i,2}(t_{f1}, v_{ref,tans}) = \mathrm{f}_1\,\delta_{crit} \tag{4.19}$$

Where, t_{fail} [s] is the time moment that an individual element fails, which can be dived by solving the differential equation of the governing motion of an ice element in the model. h [m] is the real ice thickness; N_{ref} is the amount of elements with respect to the reference measurement; and d_s is the real width of the structure. The time moment of peak load occurs in the model at an infinity velocity $v_{ref,tans}$. As approximation, the displacement of $u_{i,2}$ at the time moment that global peak load occurs t_{f1} [s] is equal to $\mathrm{f}_1\,\delta_{crit}$ [m] with f_1 selected as 0.95.

4.4. Conclusion

Three types of ice-induced vibrations by ice crushing are defined. From low to high ice speeds, these three regimes of ice-induced vibrations are divided into intermittent crushing, frequency lock-in, and continuous brittle crushing.

In addition, a phenomenological ice crushing model (Hendrikse and Metrikine, 2015) has been introduced. The method of defining the input parameters of the model, based on the reference measurement data, has also been presented.

5

DEVELOPED MODEL FOR ICE-INDUCED VIBRATIONS

5.1. Introduction

In the last chapter, the ice crushing model has been introduced. For research purpose, the structure of the original ice crushing model is modeled as a single-degree-of-freedom oscillator. However, for studying the behavior of the offshore wind turbine, a more detailed structural model is needed to include the influences of wind, current, and soil. Therefore, the focus of this chapter is on the implantation of the ice crushing model on a simplified numerical 1D beam model of the offshore wind turbine, which is shown in Figure 5.1.

In this chapter, the modeling process is first introduced in Section 5.2. Then, in Section 5.3, the natural frequency and mode analysis of this model are illustrated. Section 5.4 gives the reference properties of ice. Further, the definition of different environmental scenarios and the corresponding discussion of simulation results are presented in Section 5.5 and 5.6. Finally, the chapter ends with a conclusion in Section 5.7.

5.2. Beam model of offshore wind turbine

To capture detailed behavior of offshore wind turbine during the ice-structure interaction, a simplified 1D beam model has been built. The overview of the model is given in Figure 5.1, in which the main element of the model is an Euler-Bernoulli beam with pinned boundary condition at the bottom of the structure and the free boundary condition at the top with a point load on it.

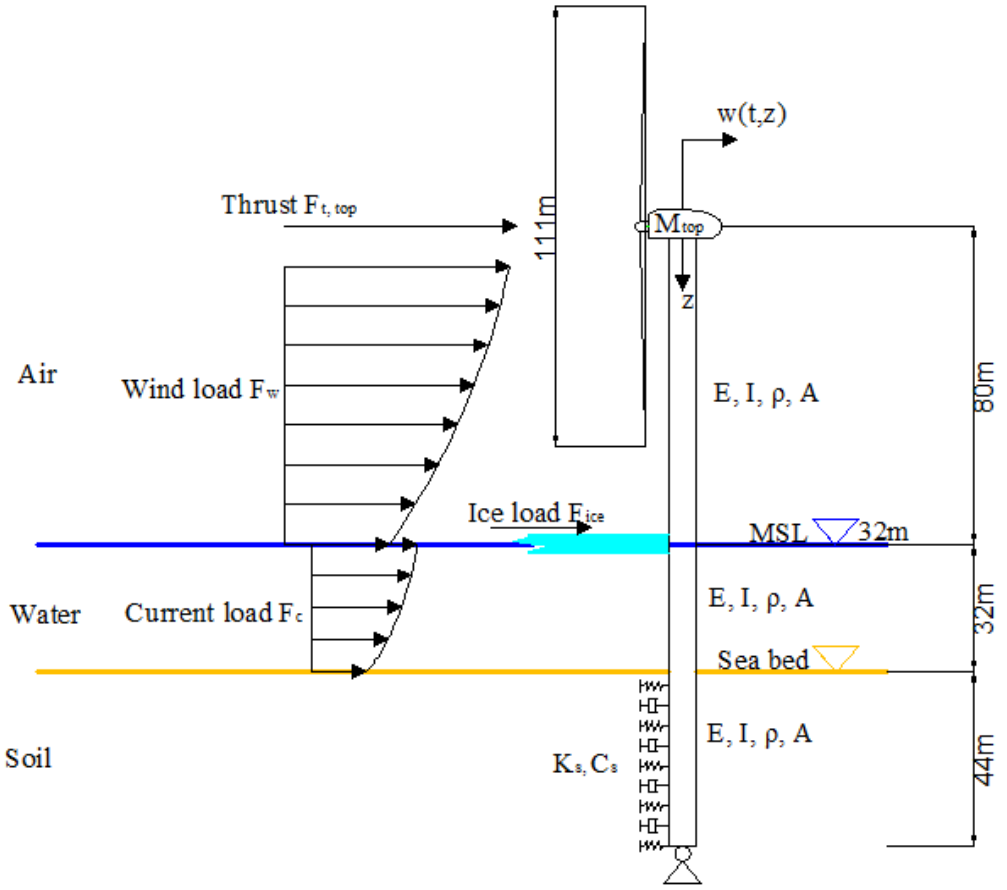

Figure 5.1: Simplified one-dimensional beam model of the offshore wind turbine.

As can be seen from the figure, the rotor-nacelle assembly is simplified as a point mass, and the load that acted on the blades is modeled as a point load by using the blade element theory in combination with momentum theory (BEM). The wind load on the tower and the current load on the support structure are acted on the structure along the z direction. Furthermore, the interaction between soil and structure is modeled by the viscous-elastic foundation, which can be obtained from the p-y curve, as shown in Figure 2.3. It is important to note that the effects of soil in this model are modeled as external loads.

The structure is modeled by using the finite differential method, which discretizes the structure into 39 segments (i.e., every segment of the structure is 4 meters long). Based on this method, the bending motion of the structure is governed by the equation:

$$\rho A \frac{\partial^2 w_i(z,t)}{\partial t^2} + C \frac{\partial w_i(z,t)}{\partial t} + EI \frac{\partial^4 w_i(z,t)}{\partial z^4} + \left(M_{top}\, g + \rho A g z_i\right) \frac{\partial^2 w_i(z,t)}{\partial z^2} = F_i(w_i, \dot{w}_i, t) \qquad (5.1)$$

Where $w_i(z,t)$ is the lateral displacement of the segment i of the wind turbine structure [m], EI is the bending stiffness of the structure [$\mathrm{N*m^2}$], M_{top} is the mass of the rotor nacelle assembly [kg], g is the gravitational constant [$\mathrm{m/s^2}$], ρ is the density of the structure [$\mathrm{kg/m^3}$], A is the cross section area [$\mathrm{m^2}$], C is the damping of the structure, z is the length from the top of the structure to the ith segment [m], and $F_i(w_i, \dot{w}_i, t)$ is the total non-linear external load that acts on the segment i [N]. From which, the segments from top to bottom of the structure are numbered as segment 1 to segment 39.

The boundary condition at the pile tip is selected to be pinned to get the structural displacement shape. Indeed, a free boundary condition would be more precise than pinned boundary condition in a real situation. However, the displacement of the pile tip in the real situation is extremely small. Thus, the pinned boundary condition would be applicable. The equation of pinned boundary condition is shown below:

$$w_{39}(L,t) = \frac{\partial^2 w_i(z,t)}{\partial z^2}\Big|_{Z=L} = 0 \tag{5.2}$$

The boundary condition at the point mass (i.e., rotor nacelle assembly) is considered as free boundary condition with a point load acting on it, which is generated from the theory of Bade Element Momentum (BEM). The boundary conditions at the top are illustrated as:

$$\frac{\partial^2 w_i(z,t)}{\partial z^2}\Big|_{Z=0} = 0$$

$$\frac{\partial^3 w_i(z,t)}{\partial z^3}\Big|_{Z=0} = F_{top}(v_{a,0}, t) - M_{top}\frac{\partial^2 w_i(z,t)}{\partial t^2}\Big|_{Z=0} \tag{5.3}$$

Based on equations (5.1)-(5.3), namely, the equations of motion and boundary conditions, the stiffness matrix and mass matrix can be derived by the finite differential method, as shown below:

Mass Matrix:

$$\mathrm{M} = \begin{bmatrix} \rho A + \frac{2m}{l} & 0 & \cdots & \cdots & \cdots & \cdots & 0 \\ 0 & \rho A & \ddots & \ddots & \ddots & \ddots & \vdots \\ \vdots & \ddots & \ddots & \ddots & \ddots & \ddots & \vdots \\ \vdots & \ddots & \ddots & \ddots & \ddots & \ddots & \vdots \\ \vdots & \ddots & \ddots & \ddots & \ddots & \ddots & \vdots \\ \vdots & \ddots & \ddots & \ddots & \ddots & \ddots & 0 \\ 0 & \cdots & \cdots & \cdots & \cdots & 0 & \rho A \end{bmatrix} \begin{bmatrix} \ddot{w}_0 \\ \ddot{w}_1 \\ \vdots \\ \vdots \\ \vdots \\ \ddot{w}_{37} \\ \ddot{w}_{38} \end{bmatrix}$$

Stiffness Matrix:

$$\mathrm{K}=\frac{EI}{l^4}\begin{bmatrix}1&-2&1&0&\cdots&\cdots&0\\-2&5&-4&1&\ddots&\ddots&\vdots\\1&-4&6&-4&1&\ddots&\vdots\\0&\ddots&\ddots&\ddots&\ddots&\ddots&0\\\vdots&\ddots&1&-4&6&-4&1\\\vdots&\ddots&\ddots&1&-4&6&-4\\0&\cdots&\cdots&0&1&-4&5\end{bmatrix}\begin{bmatrix}w_0\\w_1\\\vdots\\\vdots\\\vdots\\w_{37}\\w_{38}\end{bmatrix}+\frac{mg+\rho Agx}{12l^2}\begin{bmatrix}0&0&0&0&\cdots&\cdots&0\\1&-2&1&0&\ddots&\ddots&\vdots\\0&1&-2&1&\ddots&\ddots&\vdots\\\vdots&\ddots&\ddots&\ddots&\ddots&\ddots&\vdots\\\vdots&\ddots&\ddots&1&-2&1&0\\\vdots&\ddots&\ddots&0&1&-2&1\\0&\cdots&\cdots&0&0&1&-2\end{bmatrix}\begin{bmatrix}w_0\\w_1\\\vdots\\\vdots\\\vdots\\w_{37}\\w_{38}\end{bmatrix}$$

Damping Matrix:

The damping ratio should increase with the mode increasing and the damping ratio in the highest mode is smaller than 1. To satisfy this requirement, the damping matrix can be derived by Rayleigh damping method (J. M. J. Spijkers et al., 2005).

$$\mathrm{C}=a_0M+\mathrm{a}_1K$$

Where a_0 and a_1 are constant values, which can be determined by the first and second mode damping ratios. In this project, a_0 and a_1 are defined as 0.031 and 0.0014 respectively.

Load Matrix:

The load matrix can be defined as:

$$\mathrm{F}=\begin{bmatrix}\frac{F_{top}(v_{a,0},t)}{l}\\F_{w,1}(v_{a,1},t)\\\vdots\\F_{w,19}(v_{a,19},t)\\F_{ice}(v_{ice,20},t)\\F_{c,21}(v_{w,21},t)\\\vdots\\F_{c,27}(v_{w,27},t)\\F_{s,28}(d_{s,28},v_{s,28},t)\\\vdots\\F_{s,39}(d_{s,39},v_{s,39},t)\end{bmatrix}$$

Where, F_{top} is thrust on wind turbine [N], F_w is wind load on the tower [N], F_{ice} is ice load [N], F_c is current on the support structure [N] and F_s refers to soil effects on the foundation.

The thrust on the turbine is considered by application of the Blade Element Momentum (BEM) theory. The thrust load of turbine in different wind speed is shown in Figure 5.2.

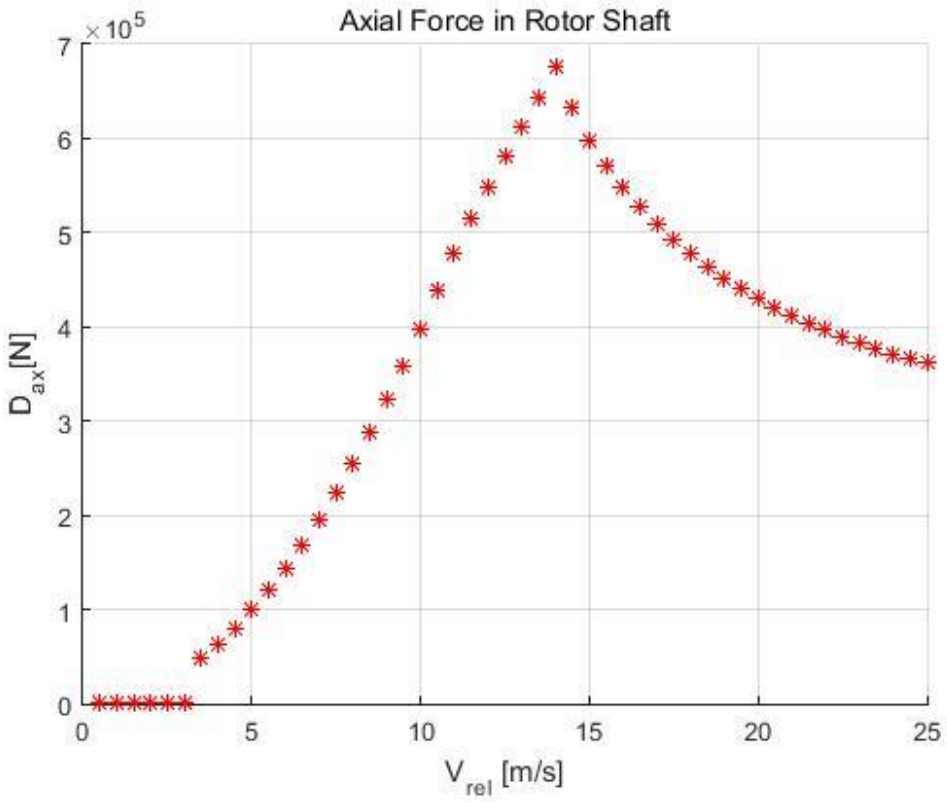

Figure 5.2: The thrust load of turbine in different wind speed, where V_{rel} is the relative velocity between wind speed and structural velocity at the top of the structure.

The wind load on the tower can be calculated by similar ways that have been illustrated in defining the design load in Chapter 3, which is given in equation (5.4):

$$F_w = \frac{1}{2}\rho_{air} D C_{D,a} (\mathrm{v}_a(z,t) - \dot{w}_i(z,t)) |(\mathrm{v}_a(z,t) - \dot{w}_{i(z,t)})| l \tag{5.4}$$

Where, ρ_{air} is the density of air [kg/m^3], D is the diameter of the structure [m], $C_{D,a}$ is the drag coefficient of the structure [-], l is segment length [m], and v is the wind velocity and can be obtained by:

$$\mathrm{v}_a = U_{10} \frac{\ln(\frac{z}{z_0})}{\ln(\frac{10}{z_0})} \tag{5.5}$$

In which, U_{10} is the wind speed at 10m height [m/s] and z_0 is the surface reference length [-].

The current load on the support structure can be calculated by the equation (5.6):

$$F_c = \frac{1}{2}\,\rho_{water}\, C_{D,f} D\,(\mathrm{u}_c(z,t) - \dot{w}_i(z,t))\left|(\mathrm{u}_c(z,t) - \dot{w}_{i(z,t)})\right| l \tag{5.6}$$

Where, ρ_{water} is the density of water [kg/m^3], $C_{D,f}$ is the drag coefficient of the structure [-], and u_c is the velocity [m/s] of water particle, which can be obtained by:

$$u_c = u_{c,0}\left(\frac{\text{water depth}+z}{\text{water depth}}\right)^{\alpha} \tag{5.7}$$

In which, $u_{c,0}$ is the surface current speed [m/s].

The ice load can be taken into account by applying the ice crushing model (Hendrikse and Metrikine, 2016).

The soil effects can be taken into account as:

$$F_s = -K_s(z)w_i(z,t) - C_s(z)\dot{w}_i(z,t) \tag{5.8}$$

In which, K_s is soil stiffness [N/m] and can be obtained from P-Y curve in Figure 2.3. C_s is soil damping, which is assumed to be of the critical value:

$$C_s = 1\% * 2 * \sqrt{\rho A l * K_s} \tag{5.9}$$

It must be mentioned that the soil resistance can be regarded as linear with the structural deflection when the structural deflection is small. To avoid long time simulation, the soil stiffness of this model is modeled as a constant value. The input values of defining external loads are given in Table 5.1:

Table 5.1: Input parameters of defining external loads

Parameter	Input Value	Dimension
ρ_{air}	1.25	kg/m^3
$C_{D,a}$	1.2	-
D	7	m
l	4	m
h_{10}	10	m
z_0	0.0002	-
ρ_{water}	1025	kg/m^3
$C_{D,f}$	1.2	-
α	1/7	-

5.3. Modal analysis

Different from the single-degree-of-freedom oscillator, the one-dimensional beam model is considered to have different modes. Therefore, frequency lock-in may occur at other modes of the structure. To have a detailed study on it, it is necessary to conduct a modal analysis of the beam.

The natural frequency and mode shape of the structure can be got by getting eigenvalues and eigenvector from the stiffness matrix (including soil stiffness) and mass matrix. The first four natural frequencies of the structure are given in Table 5.2, and Figure 5.3 shows the first four mode shapes of the structure.

Table 5.2: First four natural frequencies of the structure

Mode	Natural frequency	Dimension
1	0.18	Hz
2	1.09	Hz
3	3.23	Hz
4	6.23	Hz

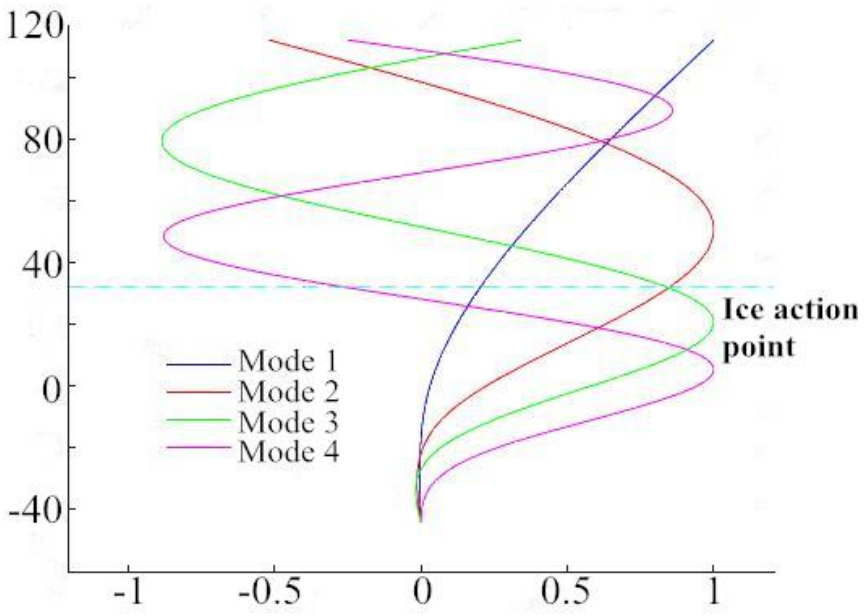

Figure 5.3: First four natural mode shapes of the structure

Based on the mode shapes of the structure, the modal mass, modal damping ratio (including soil damping) can be obtained, which are shown in Table 5.3.

Table 5.3: Modal mass, modal amplitude and modal damping ratio of the structure

Mode	Modal mass at ice action point)	Modal amplitude (at ice action point)	Modal damping ratio
1	$9.66*10^5$	0.20	1%
2	$8.73*10^5$	0.85	1.5%
3	$8.09*10^5$	0.84	4.2%
4	$8.97*10^5$	0.26	7.2%

As can be seen from the table, mode 2 and mode 3 have relatively larger modal mass and modal amplitude, which make the second and third modes easier to extract energy from the ice. However, compared to mode 2, mode 3 has larger damping ratio and natural frequency, which prevents the frequency lock-in from occurring in this mode. Therefore, from the perspective of modal analysis, it is expected that the frequency lock-in will occur in the second mode of the structure.

5.4. Ice properties

The reference ice properties that will be implemented in this model are summarized in Table 5.4. The reference width of the structure is selected to be the same as the offshore wind turbine to keep standard deviation and avoid using a large amount of ice elements in the simulation, which will consume a lot of time when applying 4th/5th order Runge-Kutta method in the Matlab iteration loop.

Table 5.4: The input reference parameters for the ice, which are used for the offshore wind turbine simulation

Parameter	Input Value	Dimension
d_{ref}	7	m
h_{ref}	0.2	m
$v_{ref,tans}$	0.001	m/s
$v_{ref,hgh}$	0.1	m/s
$F_{ref,max}$	2500000	N
$F_{ref,mean}$	500000	N
$F_{ref,mean,2}$	1500000	N
$F_{ref,std}$	50000	N
$t_{ref,peak}$	60	s
$f_{ref,peak}$	20	Hz
c_{ref}	0.3	-
f_1	0.95	-

5.5. Description of scenarios

For an offshore wind turbine, it will experience different load cases during its entire working life. To study the effects of ice-structure interaction in different load cases, eight scenarios have been defined. The load scenarios and their related parameters are given in Table 5.5.

Table 5.5: The load scenarios and its related parameters

Scenarios	Wind speed (at the top of the structure)	Ice thickness
1	Cut in wind speed	Normal
2	Rated wind speed	Normal
3	Cut out wind speed	Normal
4	extreme wind speed	Normal
5	Cut in wind speed	Extreme
6	Rated wind speed	Extreme
7	Cut out wind speed	Extreme
8	extreme wind speed	Extreme
Note		
	Cut in wind speed : 3 [m/s]	Normal: 0.2 [m]
	Rated wind speed : 14 [m/s]	Extreme: 0.67 [m]
	Cut out wind speed : 27 [m/s]	
	extreme wind speed : 39.34 [m/s]	

It must be mentioned that the wind speed that has implemented into the model is fluctuating in small amplitude around the wind speed, which is defined in Table 5.4. The surface current speed is considered as a constant value 1.94 [m/s].

5.6. Simulation results and discussion

Based on the load cases that have been defined in the last section, the corresponding ice-structure interaction simulations have been done.

Figure 5.4 - Figure 5.6 have shown the extreme ice thickness scenarios signals, which give the obtained displacement and global ice load of the offshore wind structure for ice velocities of 0.01, 0.03, and 0.1 [m/s]. The simulation results of normal ice thickness are given in Appendix.

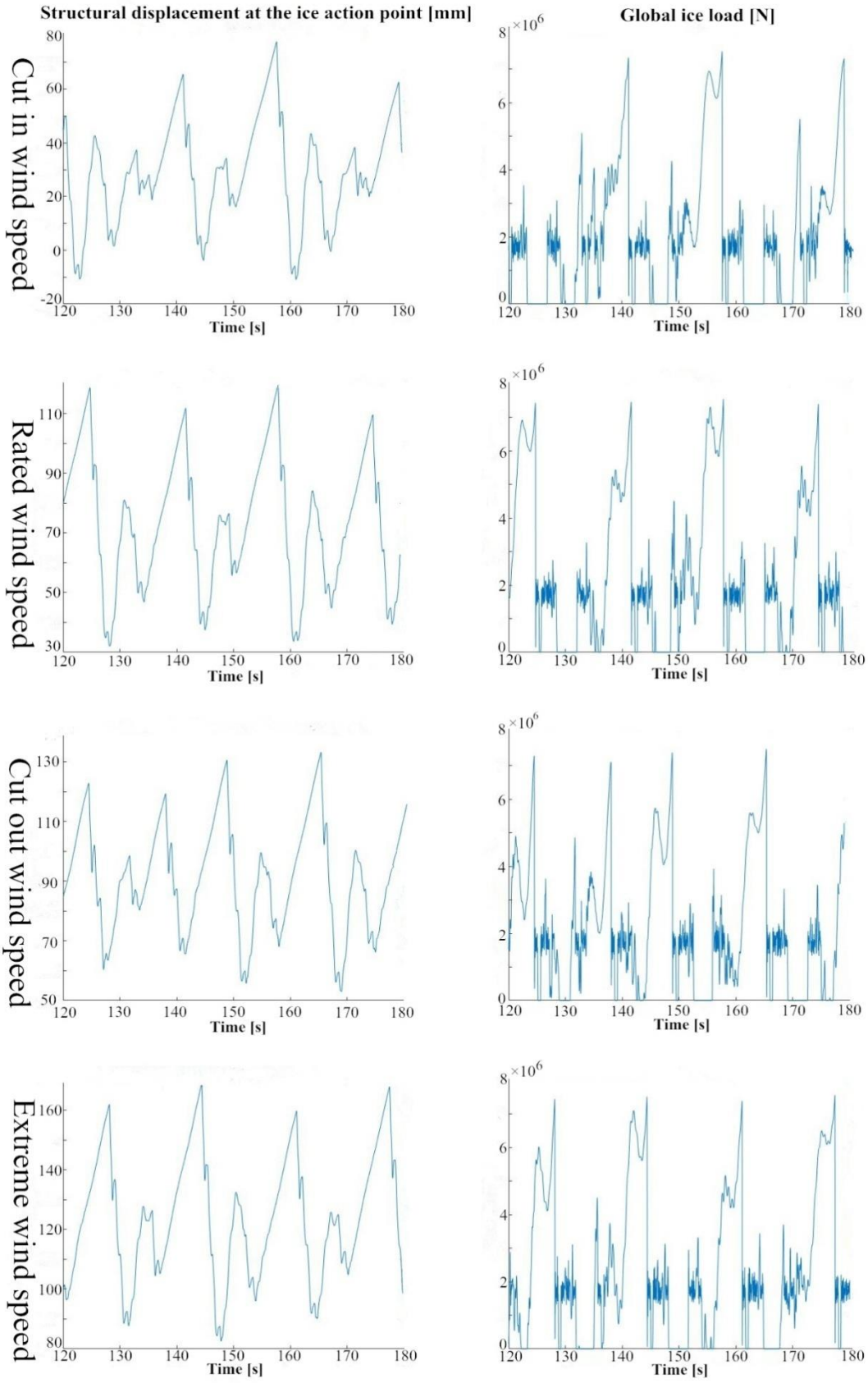

Figure 5.4: Left: Displacement of the offshore wind turbine at the ice action point for ice velocity of 0.01 [m/s]. Right: Global ice load of this ice velocity.

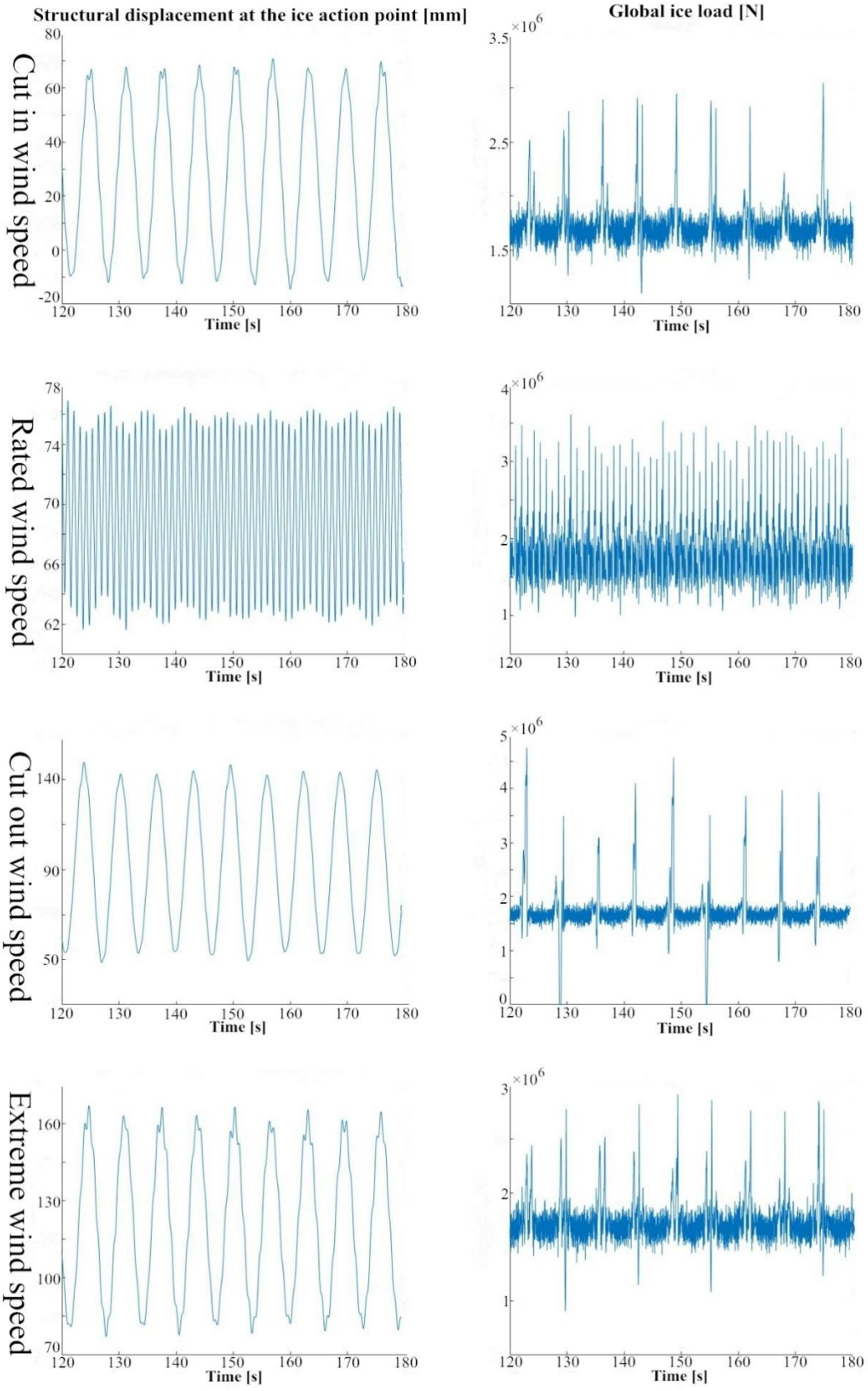

Figure 5.5: Left: Displacement of the offshore wind turbine at the ice action point for ice velocity of 0.03 [m/s]. Right: Global ice load of this ice velocity.

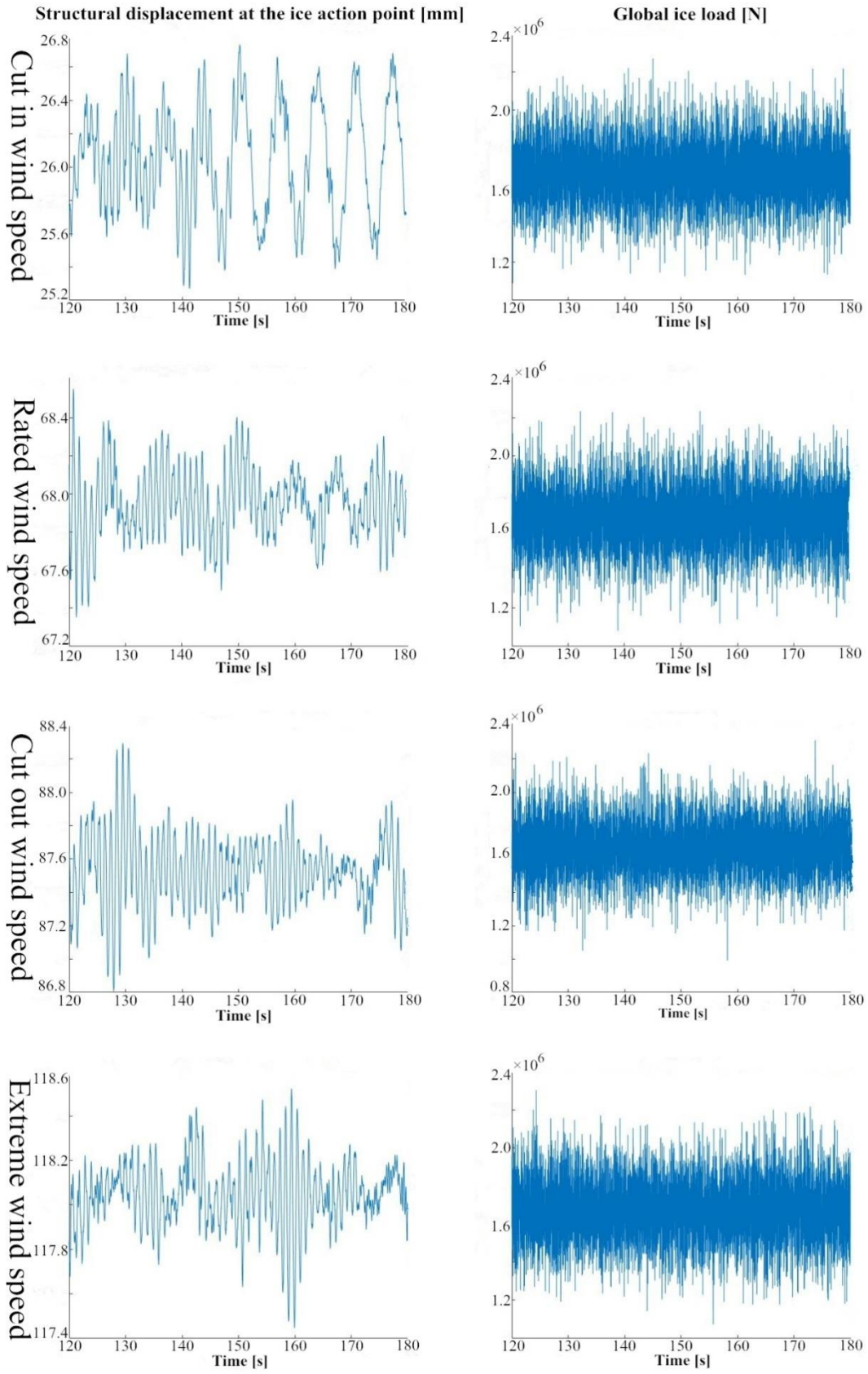

Figure 5.6: Left: Displacement of the offshore wind turbine at the ice action point for ice velocity of 0.1 [m/s]. Right: Global ice load of this ice velocity.

It can be clearly seen from these figures that intermittent crushing, frequency lock-in, and continuous brittle crushing are occurring at these three ice velocities respectively. The wind load and current loads have active effects on the mean displacement. It is interesting to see the frequency lock-in in most of the scenarios developed in the first mode rather than mode two, which is different from the obtained from the modal analysis. This illustrates the importance of including time dependence wind loads, which may cause the structural velocity non-harmonic, as shown in Figure 5.7.

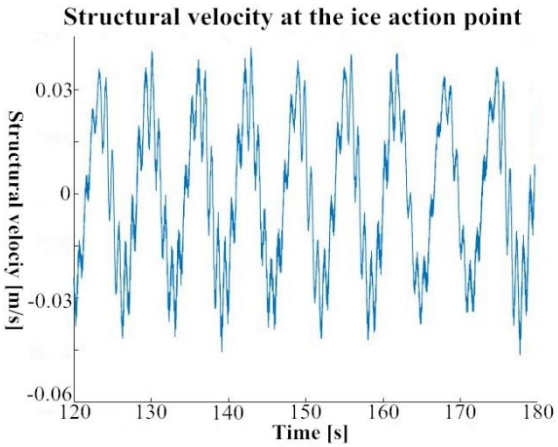

Figure 5.7: Structural velocity of first mode frequency lock-in

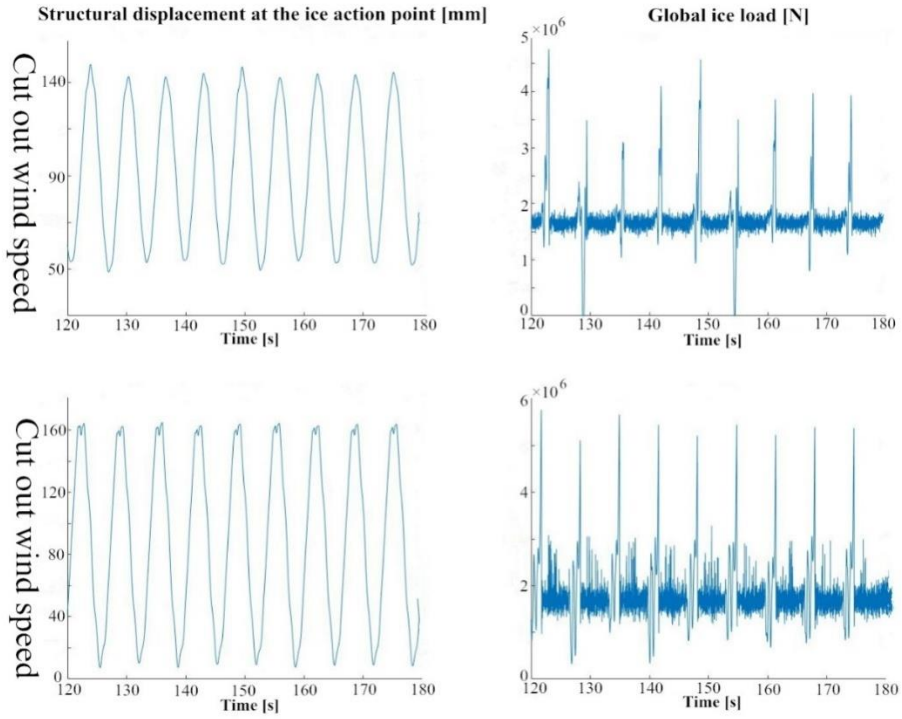

Figure 5.8: Upper: Structural displacement and global ice load of the offshore wind turbine with ice velocity of 0.03[m/s]. Lower: Structural displacement and global ice load of the offshore wind turbine with ice velocity of 0.07[m/s].

5.7. Conclusion

Based on the finite differential method, a simplified one-dimensional beam model of the monopile type offshore wind turbine has been introduced, in which the main element is an Euler-Bernoulli beam, and the relevant modal analysis has also been made.

Eight scenarios have been defined and based on these scenarios, several simulations have been conducted.

According to these simulation results, it has been found that the frequency lock-in can be developed both in first and second structural modes depending on different wind speed cases. The second mode frequency lock-in usually occurs when the wind speed is around rated wind speed, while frequency lock-in of first mode occurs in other scenarios.

The result also shows that the wind and current actions will cause a mean displacement of the structure during the ice-structure interaction. Furthermore, these loads can make the ice-structure contact lose in the regime of frequency lock-in when the ice velocity is relatively small.

Based on the simulation result, the first mode frequency lock-in is shown to be the dominant case for this structure, which will pose a potential risk to the structure. To mitigate this type of vibrations, a tuned mass damper (TMD) could be applied on the structure, which is investigated and proposed in the next chapter.

6

PHYSICAL MECHANISM AND THE MITIGATION EFFECTS OF TMD

6.1. Introduction

The previous chapter has carried out a numerical analysis of ice-induced vibrations on a monopile type offshore wind turbine, and the result shows that the high amplitude structural displacement and global ice load of first mode frequency lock-in is the main risk to the structure. To solve this problem, the mitigation solution of tuned mass damper (TMD) will be investigated in this chapter, which is shown in Figure 6.1.

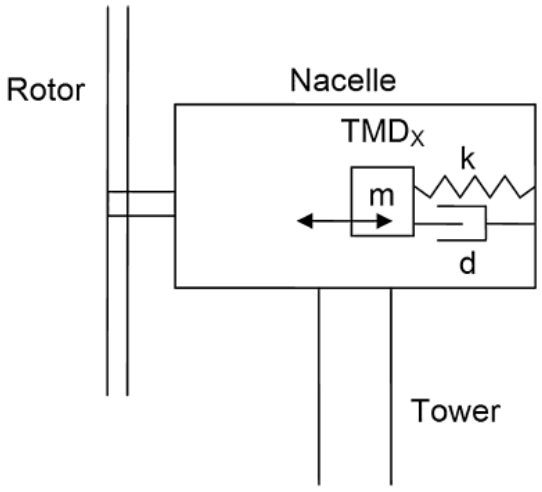

Figure 6.1: Tuned mass damper (TMD) in offshore wind turbine

In this chapter, the physical mechanism of TMD is first introduced in Section 6.2. Based on this physical mechanism, a numerical model of TMD is built and implemented in Section 6.3, and the relevant validation work on this numerical model is also presented in this section. In Section 6.4, optimized work of TMD has been done. Finally, Section 6.5 has drawn the conclusion of this chapter.

6.2. Physical mechanism of TMD

Tuned mass damper (TMD) can also be referred to as dynamic vibration absorber (DVA). Unlike other measurements of vibration mitigation, this supplementary passive device mitigates the structural vibration by absorbing the energy of the structure and has been successfully proved to be a very feasible and practical approach in civil engineering.

Normally, there are two types of TMD that are commonly implemented in civil engineering. One is a pendulum, which requires a large space to install. And the other is a sliding type of TMD, which is more compact and reliable. Considering the space limitation in the rotor nacelle assembly and the characteristics of ice-induced vibrations of the offshore wind turbine, a one-directional, sliding type of TMD is more suitable for this type of structure. The concept model of TMD device is shown in Figure 6.1, which includes the coil spring k [N/m], damping d [N*s/m], and moving mass m [kg].

6.3. Numerical model and validation

The numerical model can be built by using D. Hartog's optimal tuning formula (Den Hartog, 1956):

The optimum frequency ratio is given by

$$f = \frac{1}{1+\mu} \tag{6.1}$$

In which

Tuning frequency ratio [-] $$f = \frac{\omega_{TMD}}{\omega_{structure}} \tag{6.2}$$

TMD mass to structural mass [-] $$\mu = \frac{M_{TMD}}{M_{structure}} \tag{6.3}$$

Where, ω_{TMD} and $\omega_{structure}$ are the natural frequency of TMD and the structural frequency of ice-structure interaction respectively [rad/s]. M_{TMD} and $M_{structure}$ are the mass of TMD and offshore wind turbine respectively [kg].

Corresponding damping [N*s/m] can be defined by

$$C_{TMD} = 2M_{TMD}\,\omega_{TMD}\,\zeta_{TMD} \tag{6.4}$$

With

TMD damping ratio [-] $$\zeta_{TMD} = \sqrt{\frac{3\mu}{8(1+\mu)^3}} \tag{6.5}$$

After the numerical model of tuned mass damper has been built, the model can be implemented on the top of the offshore wind turbine beam model, and the corresponding simulation result is shown in Figure 6.2.

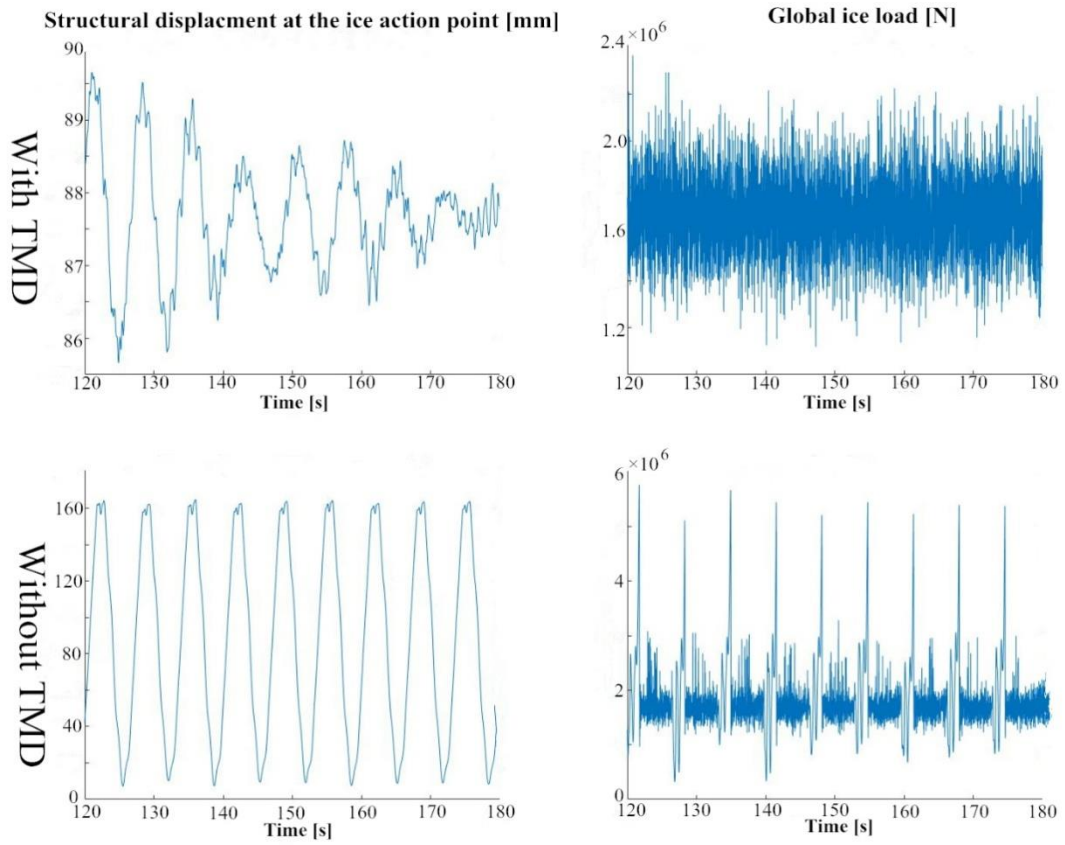

Figure 6.2: Upper: Structural displacement and global ice load of the offshore wind turbine with TMD device. Lower: Structural displacement and global ice load of the offshore wind turbine without TMD device.

As can be seen from the figure above, both structural displacements and global ice loads are significantly mitigated by the dynamic vibration absorber. Actually, it changes the way of ice-structure interaction, and the frequency lock-in is completely replaced by the continuous brittle crushing. The main reason is that the TMD can significantly reduce the structural velocities, which will increase the indentation velocities of ice and result in continuous brittle crushing.

In order to validate the effects of TMD, an absorber with extremely small mass has been tested, which is shown in Figure 6.3. The result shows that the frequency lock-in occurs again when the mass of TMD is small, which indicates that the TMD device is reliable.

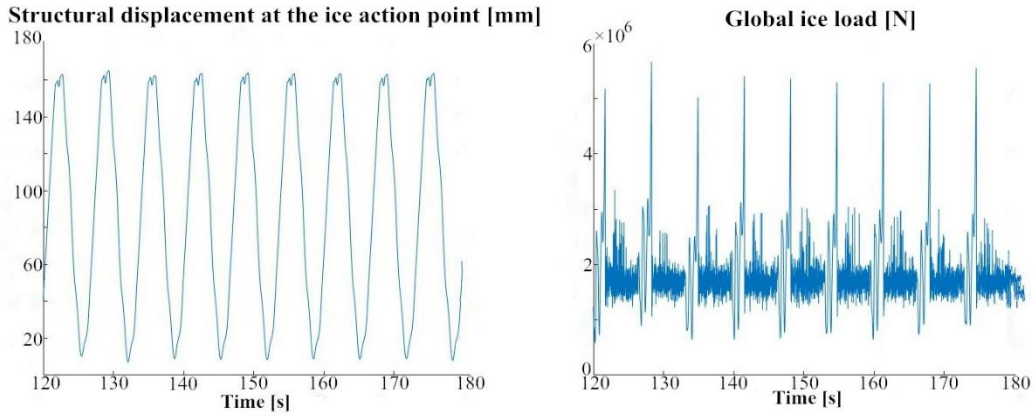

Figure 6.3: Structural displacement and global ice load of the offshore wind turbine with a TMD device that has an extremely small mass.

6.4. Mass selection

In general, the tuned mass ratio of the TMD is set between 0.5% and 2% (Yue et al., 2009). A larger mass will have an extra influence on the structural properties of the offshore wind turbine while a smaller mass will not have enough ability to absorb the energy of the structure.

However, the mitigation effects of different masses are still different in this mass ratio range, and the space limitation of the rotor nacelle assembly also has to be considered for the mass selection. Therefore, to find the optimal tuned mass ratio, several simulations have been made. The simulation results are given in Figure 6.4.

It can be clearly seen from the figure below that the structural displacement decreases with the increase of the tuned mass ratio although the differences

between them are small. The global ice loads of them do not have much difference. Therefore, it is better to use a small mass of TMD when taking economic effect into account.

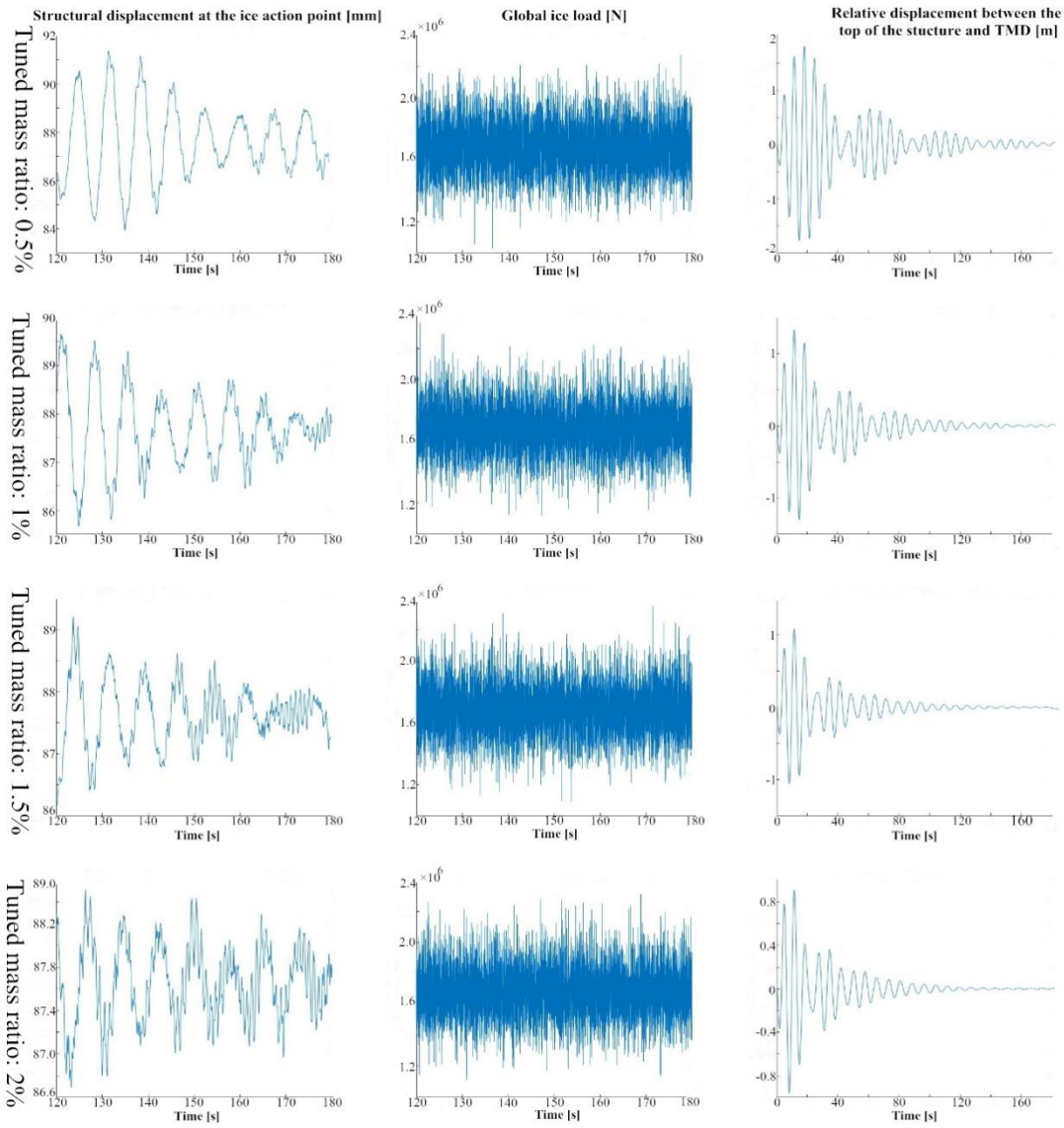

Figure 6.4: Left: Structural displacements at the ice action point for different masses of the TMD. Centre: Global ice load for different masses of the TMD. Right: Relative displacements between the TMD and the rotor nacelle assembly of the structure for different masses of the TMD.

However, the relative displacements between the TMD and the rotor nacelle assembly are also an important factor that needs to be considered. As can be seen from the figure above, the relative displacements are quite large at the beginning when the load starts to act on the structure, and this effect gradually weakened with the increase of tuned mass ratio. Since the relative displacement of 1.5% tuned mass ratio and 2% tuned mass ratio are more acceptable than the other

two mass ratios and the difference between them are small. Therefore, by taking all the factors into account, a 1.5% tuned mass ratio TMD device is recommended to be applied to this project.

6.5. Conclusion

A theory for the explanation of the physical mechanism of the tuned mass damper (TMD) has been presented. Base on this theory the numerical model of TMD has been implemented. The corresponding simulations have been conducted as well. From the results of simulations, it has been found that the TMD device can absorb most of the energy of the offshore wind turbine. Both structural displacements and global ice loads are significantly mitigated by the dynamic vibration absorber, and the frequency lock-in is replaced by continuous brittle crushing.

Furthermore, to optimize the mitigation effects, several simulations have been done based on different tuned mass ratio. By taking mitigation effects, space limitation, and economic effects into account, a 1.5% tuned mass ratio TMD device is proved to be an applicable choice of the investigated structure.

The work of this project is ended in this chapter. In the next chapter, some works that could be studied in the future are introduced.

7

FURTHER WORKS

7.1. Introduction

The current chapter puts emphasis on further works that could be done in the future. Some examples and some directions will be presented in this chapter.

In Section 7.2, the experimental validation work has been introduced. The influence of ice properties' variation is proposed in Section 7.3. Then, the ice-structure interaction in multi-legged structures is described in Section 7.4. Finally, the other type of dynamic vibration absorbers is given in Section 7.5. The conclusion of this chapter is summarized in Section 7.6.

7.2. Validation by experiment

In the previous chapters, the analyses of ice-induced vibrations on an offshore wind structure and the corresponding mitigation solution by means of tuned mass damper (TMD) have already been done numerically. However, these simulation results have insufficient support from test results. Hence, there is a need to carry out an experiment validation.

The experiment could be set in an ice and wind producing towing tank, and the dimensions of the beam and the environmental inputs could be set by applying the scaling laws. The thrust on the turbine could be replaced by a point force, which acts on the top of the structure, and the foundation could be fixed to replace the soil effects.

7.3. Variation of ice properties

In this thesis, most of the ice properties are considered to be constant in the numerical model. However, in reality, ice properties are changing over time. For example, the ice velocity and the ice thickness are not always keeping constant, nor are the grain size, temperature, salinity, and porosity of the ice constant, which will directly affect the strength of the ice. For getting a realistic load signal of the ice-structure interaction, the variation of ice properties should be taken into account as well.

To solve this problem, the ice properties can be considered in three parts: ice velocity, ice thickness, and ice strength. The ice strength can be treated as random variables, and based on this distribution, the ice elements can be modeled differently along the structure, which has already been included in the ice-crushing model (Hendrikse and Metrikine, 2015). The ice thickness and velocities can be considered to form a certain distribution on the basis of the statistical results obtained from the field test. Then, these two variables can be solved in a probabilistic way.

7.4. Multi-legged structures

In this thesis, the monopile type foundation has been selected. However, due to the unfavorable soil conditions in Bohai Bay, various foundations will be applied in this area such as jacket and compliant tower. Therefore, the investigation of the interaction between ice and multi-legged structure is also necessary to be conducted in further work.

For multi-legged structure, the ice splitting needs to be considered. The ice-structure interaction between closely spaced legs or piles will cause ice jamming on the structure. According to the study of Timco and Pratte (1985), the ice rubble will be generated when the pile spacing is smaller than six pile diameters. Thus, to capture the effects of ice-structure interaction of multi-legged structure, an extension work is needed.

7.5. Tuned liquid damper

In this thesis, the vibration mitigation effects of tuned mass damper (TMD) have been discussed. However, the tuned mass damper is not the only vibration absorber that has been applied in civil engineering. Other solutions such as tuned liquid damper (TLD) are also widely used.

A TLD is a device in which water is confined in a container that uses the sloshing energy of the water to reduce the dynamic response of the system when the system is subjected to excitation (Figure 7.2), which has also been found to be very effective in canceling vibrations. Furthermore, TLD has been proved to have a better performance than TMD for low-frequency vibrations (Mondal et al., 2014). Since the first mode frequency lock-in for an offshore wind turbine always develops at a low frequency, it is important to have a further study on the effects of TLD.

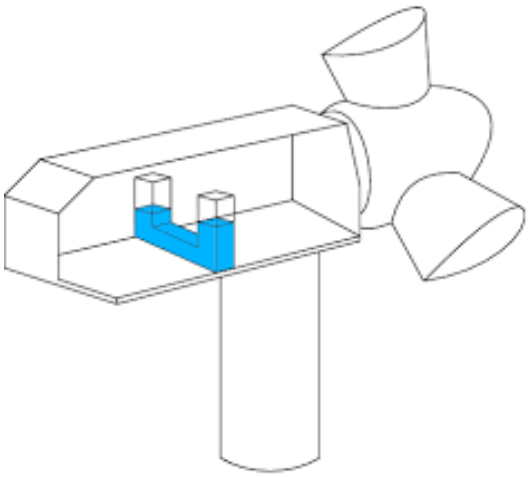

Figure 7.2: Tuned liquid damper in wind turbine

7.6. Conclusion

Several additional works have been proposed in this chapter.

A validation experiment of ice-induced vibrations on an offshore wind turbine model is presented and discussed. In addition, the way to deal with the variation of ice properties has been illustrated. Finally, some other types of foundations of the offshore wind turbine such as multi-legged structures and other types of vibration mitigation devices including tuned liquid damper (TLD) have been identified.

8

CONCLUSION

The main purpose of this thesis is to study the mitigation effects of tuned mass damper (TMD) on ice-induced vibration. To achieve this goal, the environmental data are first collected and processed. In accordance with the data, the offshore wind turbine is designed and modeled. On the basis of the model, the ice-structure interaction and the mitigation effects of TMD have been analyzed numerically.

In Chapter 2, the background of this project is first introduced, which shows that China is experiencing a rapid development of offshore wind market. Then, the environmental data of this project area have been summarized and processed.

Chapter 3 is mainly concentrated on the preliminary design of the offshore wind turbine. And then the structure is considered as a cylinder with a 7-meter diameter. Therefore, the primary purpose of the design is to determine the total length of the structure. Based on extreme load cases and soil conditions, the total length of the structure has been obtained, and the corresponding design check has been done as well.

Based on indentation velocities, three regimes of ice-induced vibrations are first introduced in Chapter 4. Then, a phenomenological ice crushing model has been illustrated in this chapter.

In line with the structural parameters and environmental data, a one-dimensional beam model has been built by finite differential method in Chapter 5. According to the simulation results, both first mode and second mode frequency lock-in can be developed during the ice-structure interaction. It has also shown that the wind and current loads may cause the structure to lose contact with the ice in the regime of first mode frequency lock-in when the ice

speed is relatively small, and this phenomenon will disappear with the increase of ice velocities.

As a mitigation solution of the ice-induced vibration, the tuned mass damper (TMD) has been proposed and analyzed numerically in Chapter 6. Based on simulation results, it can be concluded that the TMD device can effectively mitigate ice-induced vibration. In fact, the frequency lock-in is replaced by continuous brittle crushing. Furthermore, by taking multi-factors into account, a 1.5% tuned mass ratio is shown to be at suitable value for the investigated structure.

Finally, several further works have been summarized in Chapter 7, including experimental validation work, variation of ice properties, ice-induced vibration on multi-legged structures, and the mitigation effects of tuned liquid damper (TLD).

REFERENCES

API RECOMMENDED PRACTICE 2A-WSD (2000). American petroleum institute-Recommended Practice for Planning, Designing and Constructing Fixed Offshore Platforms—Working Stress Design, pages 64-66.

Blenkarn, K. A. (1970). Measurements and analysis of ice forces on Cook Inlet structures. In Proceedings of the Second Annual Offshore Technology Conference, volume II, pages 365-378, Houston, Texas.

China National Energy Administration. (2016). the 13th Five-Year Plan for wind power development, page 7 (in Chinese).

Den Hartog, J.P. (1956). Mechanical Vibrations, 4th ed. McGraw-Hill, New York.

DNV-OS-J101 (2013). Design of Offshore Wind Turbine Structures.

Dorival, O., Metrikine, A.V., and Simone, A. (2008). A lattice model to simulate ice-structure interaction. In Proceedings of the ASME International Conference on Offshore Mechanics and Arctic Engineering, volume 3, pages 989-996, Estoril, Portugal.

Engelbrektson, A. (1977). Dynamic ice loads on lighthouse structures. Proc. 4th Int. Conf. on Port and Ocean Eng. Under Arctic Conditions, St. John's, Canada, vol. 2, pp. 654-864.

Gautier, D.L., Bird, K.J., Charpentier, R.R., Grantz, A., Houseknecht, D.W., Klett, T.R., Moore, T.E., Pitman, J.K., Schenk, C.J., Schuenemeyer, J.H., Sørensen, K., Tennyson, M.E., Valin, Z.C., and Wandrey, C.J. (2009). Assessment of undiscovered oil and gas in the arctic. Science, 324(5913): 1175-1179.

General Electric Company (2005). 3.6MW Offshore Series Wind Turbine.

GL (2012). Guideline for the Certification of Offshore Wind Turbines.

Gürtner, A., Bjerkas, M., Forsberg, J., and Hilding, D. (2010). Numerical modelling of a full scale ice event. In Proceedings of the 20th IAHR International Symposium on Ice, page 16, At Lathi, Finland.

Gu X. (2008). Suggestions for Shanghai's wind farm planning and development. Water Resources Planning and Design. 1: 8–10 (in Chinese).

Hendrikse, H. and Metrikine, A. (2015). Interpretation and prediction of ice induced vibrations based on contact area variation. Int. J. Solids Struct., 75-76:336-348.

Hendrikse, H. and Metrikine, a. (2016). Ice-induced vibration and ice buckling. Cold Reg. Sci. Technol., 131:129-141.

Huang, Y., Shi, Q., and Song, A. (2007). Model test study of the interaction between ice and a compliant vertical narrow structure. Cold Reg. Sci. Technol., 49: 151-160.

ISO19906 (2010). Petroleum and natural gas industries-arctic offshore structures.

Jefferies, M.G. and Wright, W.H. (1988). Dynamic response of 'Molikpaq' to ice-structure interaction. In Proceedings of the Seventh International Conference on Offshore Mechanics and Arctic Engineering, volume 4, pages 201-220, Houston, Texas.

Kärnä, T. and Muhonen, A. (1990). Preliminary results from ice indentation tests using flexible and rigid indentors. In proceedings of the Tenth IAHR International Symposium on Ice, volume 3, pages 261-275, Espoo, Finland.

Kärnä, T. (1992). Aprocedure for dynamic soicl-structure-ice interaction. In Proceedings of the Second International Offshore and Polar Engineering Conference, pages 764-771, San Francisco, California.

Kärnä, T. and Jchmann, P. (2003). Feld observations on ice failure modes. In Proceeding of the 17th Internatioonal Conference on Port and Ocean Engineering under Arctic Conditions, pages 839-848, Trondheim, Norway.

Kry, P. R. (1978). A statistical prediction of effective ice crushing stress on wide structure. Proc., 4th IAHR Symp. on Ice Problems, Delft, The Netherlands 33–47.

Määttänen, M. (1978). On conditions for the rise of self-excitied ice-induced autonomous oscillations in slender marine pile structures. Research Report No.25, Winter Navigation Research Board.

Määttänen, M. (1983). Modelling the interaction between ice and structures. In Proceedings of the Seventh International Conference on Port and Ocean Engineering under Arctic Conditions, volume 2, pages 745-759, Helsinki, Finland.

Matlock, H., Drawkins, W. P., and Panak, J. J. (1969). A model for the prediction of ice-structure interaction. In Proceedings of the First Annual Offshore Technology Conference, Pages 687-694, Houston, Texas.

Mondal, J., Nimmala, H., Abdulla, S., and Tafreshi, S. (2014). Tuned liquid damper. In Proceedings of the 3rd International Conference on Mechanical Engineering and Mechatronics Prague, Czech Republic, August 14-15, 2014 Paper No. 68.

Pang, W. and Wang, X. (2010). Research and Analysis of Capability of Structure of Offshore Wind Turbine. Harbin Engineering University Y1809058 pp.23-58 (in Chinese).

Peyton, H.R. (1968). Sea ice forces. In Ice Pressure Against Structures, compiled by L. Gold and G. Williams, NRC Techn. Memo No.92, Ottawa, Canada.

Saeji, H., Hiratama, K., Kawasaki, T., Akagawa, S., Kato, K., Kamesaki, K. Saka, K., and Kurokawa, A. (1996). JOIA project of study on ice load. In Proceedings of the 13th IAHR International Symposium on Ice, volume 1, pages 17-27, Beihing, China.

Schwarz, J. and Jochmann, P. (2001). Ice force measurements within the LOLEIF-project. In Proceedings of the 16th IAHR International Symposium on Ice and Its Action on Hydraulic Structures, page 12, Reykjavik, Iceland.

Sodhi, D. S., Morris, C. (1984). Ice forces on rigid, vertical, cylindrical structures. CRREI. Report 84-133, December 1984.CT

Sodhi, D. S. (2001). Crushing failure during ice-structure interaction. Eng. Fract. Mech., 68: 1889-1921.

Spijkers, J.M.J., Vrouwenvelder, A.W.C.M., Klaver. E.C. (2005). Structural Dynamic CT4140. Delft University of Technology-Faculty of Civil Engineering and Geosciences. Pages: 48-51.

Toyama, Y., Sensu, T., Minami, M., and Yashima, N. (1983). Model tests on ice-induced selft-excited vibration of cylindrical structures. In Proceedings of the eventh International Conference on Port and Ocean Engineering under Arctic Conditions, volume 2, pages 834-844, Helsinki, Finland.

Tsuchiya, M., Kanie, S., Ikejiri, K., Yoshida, A., and Saeki, H. (1985). An experimental study on ice-structure interaction. In Proceedings of the Seventeenth Annual Offshore Technology Conference, pages 321-327, Houston, Texas.

Wang, N. and Wu, J. (2005). Research on marine engineering environment and feasibility of pile foundation at the Bohai Bay west area. Ocean University of China Y828801 pp.5-46 (in Chinese).

Xu, N., Yue, Q.J., Guo, F.W., and Qu, Y (2011). Mitigation of Ice-induced Vibrations by Adding Cones. International Journal of Offshore and Polar Engineering, Vol. 21, No. 1, March 2011, pp. 56 – 60.

Yang, G.J. (2000). Bohai Sea ice condition. J. of Cold Region Engineering 14(2): 54-67.

Yue, Q., Zhang, X., Bi, X., and Shi, Z. (2001). Measurements and analysis of ice induced steady state vibration. Prod 16th Int. Conf. Port Ocean Eng. under Arctic. Cond. Ottawa, Canada.

Yue, Q., Bi, X, Zhang, X., and Kärnä, T. (2002). Dynamic ice forces caused by crushing failure. In Proceedings of 16th IAHR International Symposium on Ice, volume 3, pages 231-237, Dunedin, New Zealand.

Yue, Q.J. and Li, L. (2003). Ice problems in Bohai Sea oil exploitation. In Proceedings of the 17th International Conference on Port and Ocean Engineering under Arctic Conditions, page 13, Trondheim, Norway.

Yue, Q., Bi, X., Zhang, X., and Kärnä, T. (2007). Ice force spectrum on narrow conical structures. Cold Reg. Sci. Technol., 49:161-169.

Yue, Q., Guo, F. W., and Kärnä, T. (2009). Dynamic ice force of slender vertical structures due to ice crushing. Cold Reg. Sci. Technol. 56: 77-83.

Yue, Q., Zhang, L., Zhang, W.S., and Kärnä, T. (2009). Mitigating ice-induced jacket platform vibrations utilizing a TMD system. Cold Reg. Sci. Technol., 56:84-89.

Zhang, D., Zhang, X. L., He, J. K., and Chai, Q. M. (2011). Offshore wind energy development in China: Current status and future perspective. Renewable and Sustainable Energy Reviews. 15: 4673-4684.

APPENDIX

The simulation results of ice-induced vibration for different scenarios are summarized in this part.

Scenario 1: Extreme ice thickness (0.67m) with Cut-in wind speed (3m/s). Ice velocities: 0.01, 0.03, and 0.1 [m/s].

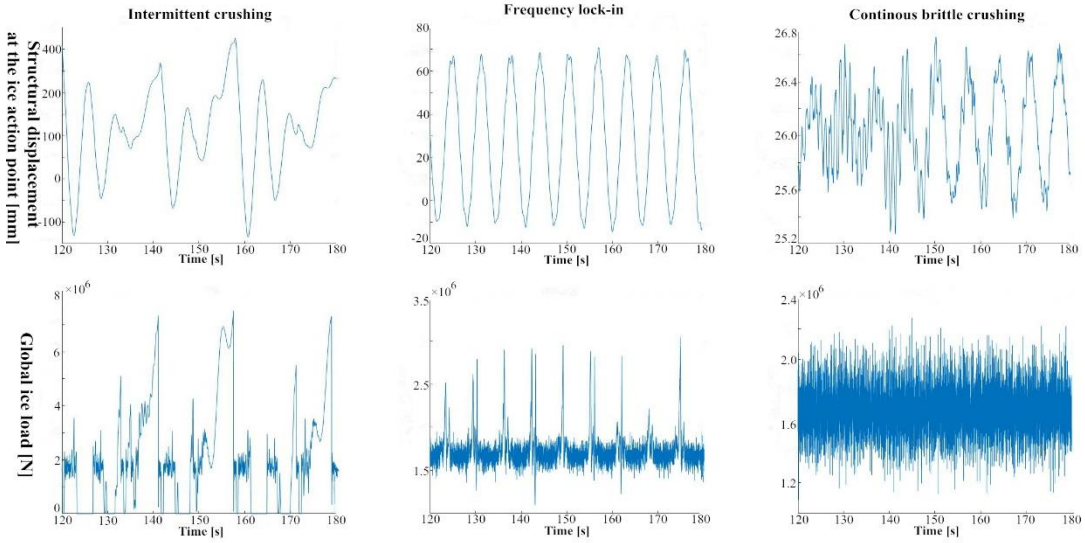

Scenario 2: Extreme ice thickness (0.67m) with Rated wind speed (14m/s). Ice velocities: 0.01, 0.03, and 0.1 [m/s].

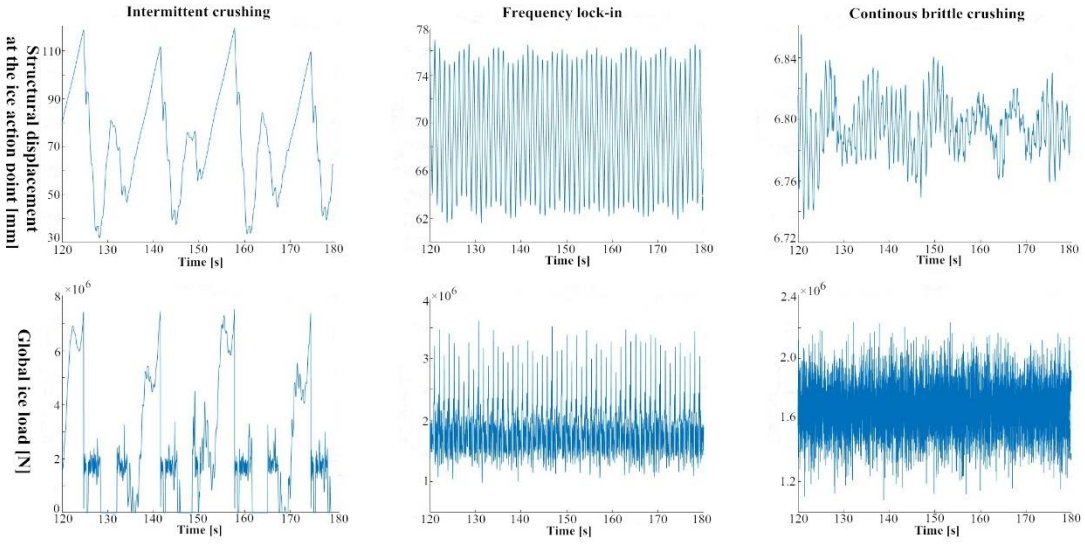

Scenario 3: Extreme ice thickness (0.67m) with Cut-out wind speed (27m/s). Ice velocities: 0.01, 0.03, and 0.1 [m/s].

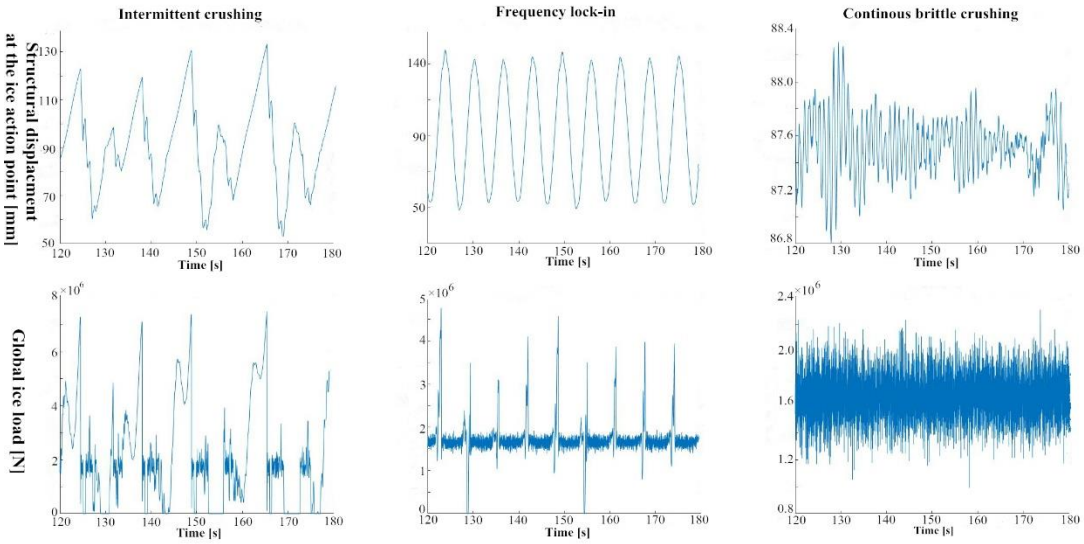

Scenario 4: Extreme ice thickness (0.67m) with Extreme wind speed (39.34m/s). Ice velocities: 0.01, 0.03, and 0.1 [m/s].

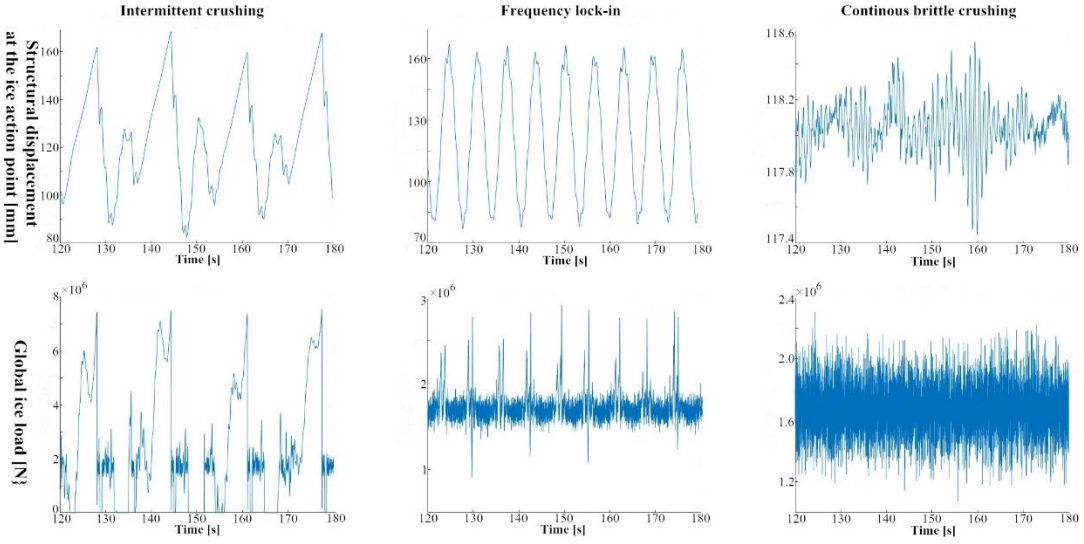

Scenario 5: Normal ice thickness (0.2m) with Cut-in wind speed (3m/s). Ice velocities: 0.005, 0.03, and 0.1 [m/s].

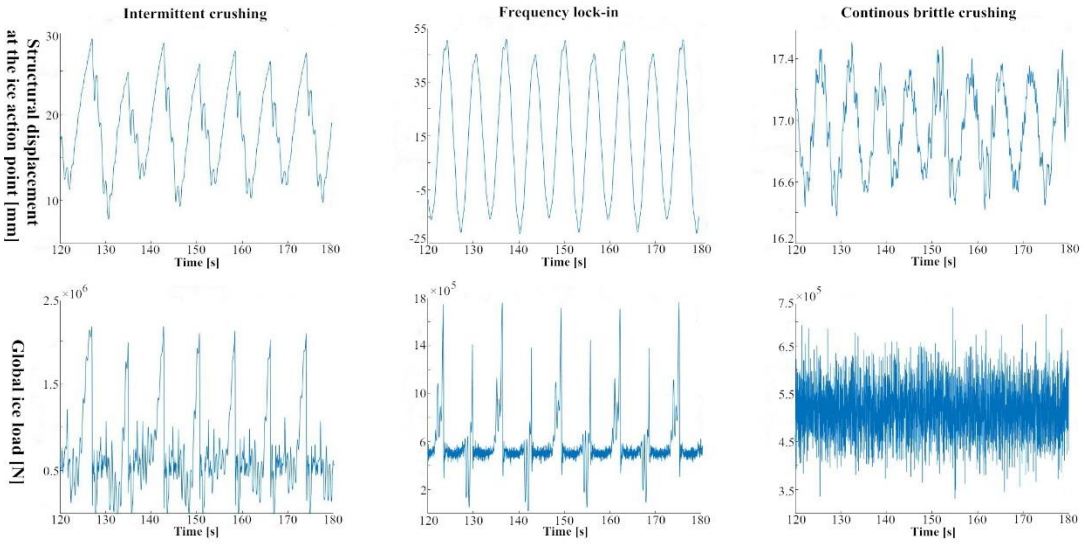

Scenario 6: Normal ice thickness (0.2m) with Rated wind speed (14m/s). Ice velocities: 0.005, 0.03, and 0.1 [m/s].

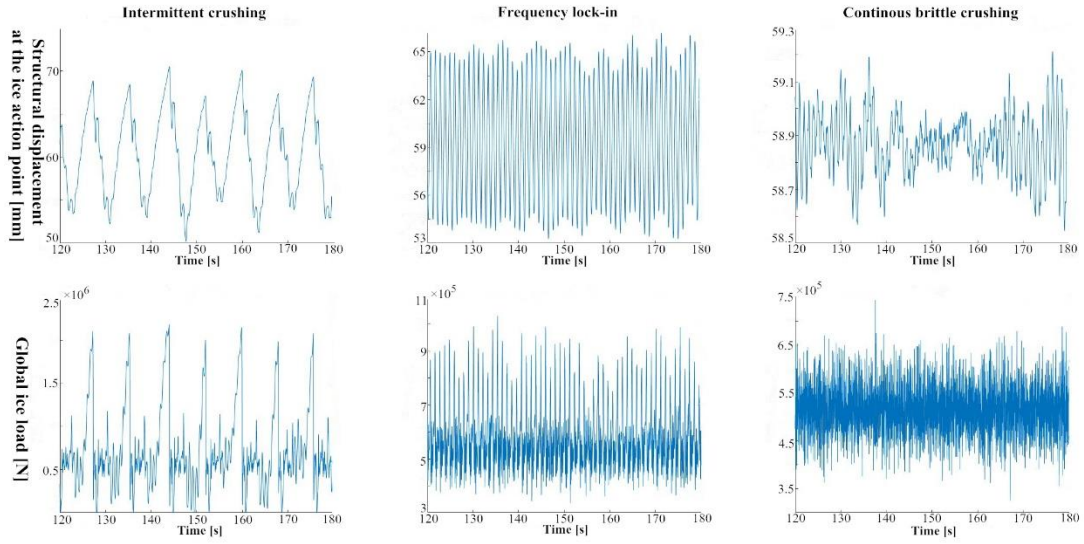

Scenario 7: Normal ice thickness (0.2m) with Cut-out wind speed (27m/s). Ice velocities: 0.005, 0.03, and 0.1 [m/s].

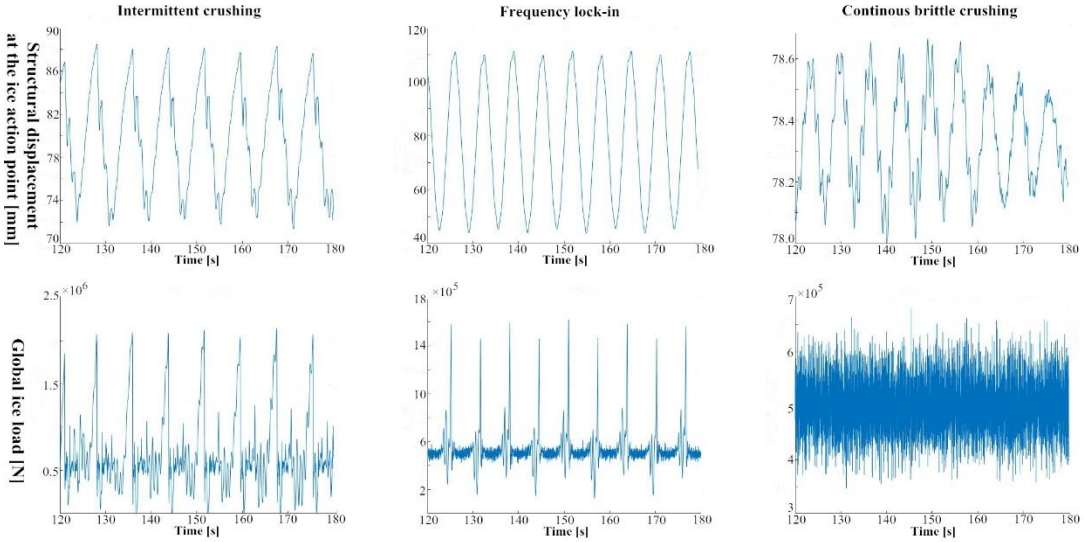

Scenario 8: Normal ice thickness (0.2m) with Extreme wind speed (39.34m/s). Ice velocities: 0.005, 0.03, and 0.1 [m/s].

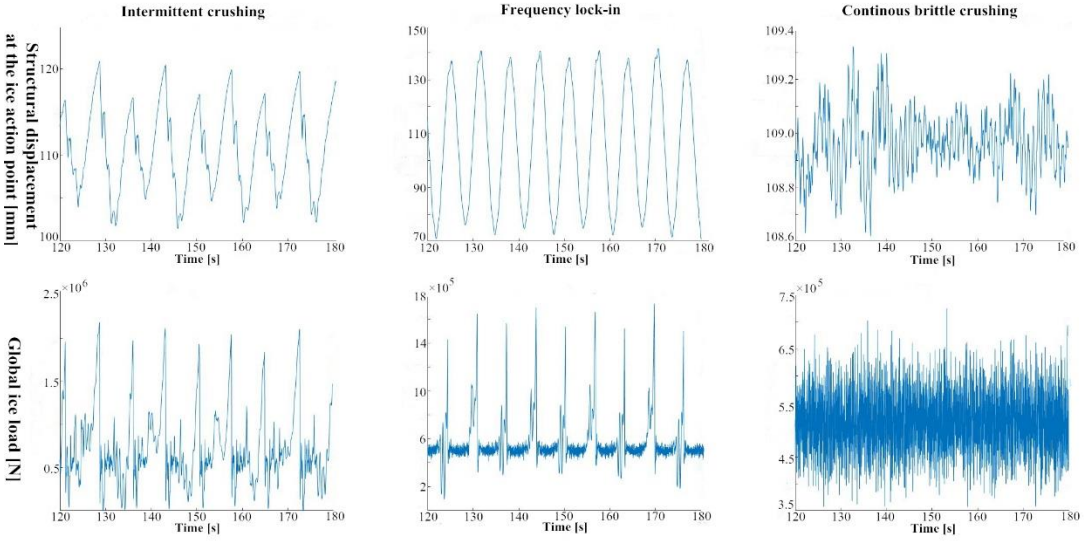

ACKNOWLEDGEMENTS

The journey of my two years of master's degree study in TU Delft has come to an end. It was an amazing experience when looking back at the time that I lived and studied here, which I will treasure forever. Honestly speaking, I really feel myself to be lucky to have an opportunity to study in TU Delft. The high quality of education, the high-standard teachers, and the abundant campus culture push me to become better and better.

The first people I would like to say thanks is my main supervisor, Hayo. Thank you for the guidance and advices on my thesis. You are such a nice teacher who is always patient to help me solve the problems encountered in my thesis no matter how busy you are. I'm really proud of having such an excellent supervisor. I have learned a lot from you, not only the knowledge, but also the way of thinking and problem solving. Our weekly meetings and countless emails have resulted in a great friendship between us which I really treasure.

I would also like to thank my chairman Jeroen for helping me find such a good thesis topic. Thank you for your tutorial while Hayo was on holiday and that helps me a lot for the progress of my thesis.

My friends, I would like to say thanks to you guys. Thank you for the companionship that you guys gave to me. Actually, it is the first time that I left my hometown and I have encountered a lot of problems and difficulties. Without you guys, I could hardly keep going on my life here.

Finally, my parents, I would like to express my heart-felt thanks to you for creating the possibilities to let me have a chance to go abroad and look at this world, and for your unwavering support and trust, no matter what difficulties I encountered.